SC5211.3FR

SC5211.3FR

Copy No. 76

MECHANISMS BY WHICH HUMIDITY ALTERS DUCTILITY

FINAL REPORT FOR THE PERIOD April 15, 1979 through April 14, 1982

CONTRACT NO. N00014-79-C-0334

Prepared for

Office of Naval Research
800 N. Quincy Street
Arlington, VA 22217

W.L. Morris, M.R. James, R.V. Inman
Principal Investigators

JUNE 1982

Research was sponsored by the Office of Naval Research under Contract No. N00014-79-C-0334, project number NR 036-134 (471).

Approved for public release; distribution unlimited

Rockwell International
Science Center

UNCLASSIFIED

SECURITY CLASSIFICATION OF THIS PAGE (When Data Entered)

REPORT DOCUMENTATION PAGE		READ INSTRUCTIONS BEFORE COMPLETING FORM
1. REPORT NUMBER	2. GOVT ACCESSION NO. AD-A116030	3. RECIPIENT'S CATALOG NUMBER
4. TITLE (and Subtitle) MECHANISMS BY WHICH HUMIDITY ALTERS DUCTILITY		5. TYPE OF REPORT & PERIOD COVERED Final Technical Report for the period 4/15/79-4/14/82
		6. PERFORMING ORG. REPORT NUMBER SC5211.3FR
7. AUTHOR(s) W.L. Morris, M.R. James and R.V. Inman		8. CONTRACT OR GRANT NUMBER(s) N00014-79-C-0334
9. PERFORMING ORGANIZATION NAME AND ADDRESS Rockwell International Science Center 1049 Camino Dos Rios Thousand Oaks, California 91360		10. PROGRAM ELEMENT, PROJECT, TASK AREA & WORK UNIT NUMBERS NR 036-134 (471)
11. CONTROLLING OFFICE NAME AND ADDRESS Department of the Navy Office of Naval Research Arlington, VA 22217		12. REPORT DATE June 1982
		13. NUMBER OF PAGES 76
14. MONITORING AGENCY NAME & ADDRESS(if different from Controlling Office)		15. SECURITY CLASS. (of this report) UNCLASSIFIED
		15a. DECLASSIFICATION/DOWNGRADING SCHEDULE

16. DISTRIBUTION STATEMENT (of this Report)

Approved for public release; distribution unlimited

17. DISTRIBUTION STATEMENT (of the abstract entered in Block 20, if different from Report)

18. SUPPLEMENTARY NOTES

19. KEY WORDS (Continue on reverse side if necessary and identify by block number)

Ductility, surface properties, corrosion environments, fatigue, cracking, fatigue properties, surface defects, crack initiation, aluminum alloys, plastic theory.

20. ABSTRACT (Continue on reverse side if necessary and identify by block number)

The effects of atmospheric humidity and of internal hydrogen on localized surface ductility of a Al 2219-T851 alloy have been characterized. A reference gauge technique was used to measure the peak tensile plastic strains which develop during fatigue within individual grains at the surface of the alloy. These are sensitive to environment and can exceed 0.5%, even when the bulk deformation is linearly elastic. The average strain at the surface is controlled by the subsurface, resulting in a mixed pattern of

DD FORM 1 JAN 73 1473 EDITION OF 1 NOV 65 IS OBSOLETE

UNCLASSIFIED

SECURITY CLASSIFICATION OF THIS PAGE (When Data Entered)

tensile and compressive strains from grain to grain. The hysteresis loops open more rapidly with fatigue within grains having large distances of slip between boundaries at the surface. Constituent particles are fractured when the width of the local stress-strain hysteresis loop increases to a critical value. A simple strain energy criterion for particle fracture is used to model the probability of particle fracture from the accumulation of slip from the particle to the grain boundary. Agreement is achieved with experimental data by assuming that environmental factors alter the local ductility of the matrix material within individual grains, but not the particle fracture surface energy. Ambient humidity is found to decrease the rate of fatigue induced opening of the local stress-strain hysteresis loops. Internal hydrogen increases the rate. Concomitantly, substantially more particles are fractured in an alloy containing even small amounts (1<ppm) of internal hydrogen.

The local ductility of the surface also plays a role in the rate of propagation of short surface cracks. Crack tip plasticity is much larger than the strains involved in crack initiation, and the sensitivity to environment is partially reversed for crack growth. By measuring crack tip opening displacements we find that both internal hydrogen and ambient humidity reduce the ductility of the material at the tip of small surface cracks. This leads to accelerated growth rates. It appears that at small strains (<0.3%) hydrogen increases the local ductility of the 2219 matrix material, whereas at large strains (>1%) it decreases ductility. The observation that humidity and internal hydrogen change the ductility in opposite directions at small strains provides indirect evidence that hydrogen does not penetrate the oxide surface barrier until a crack is formed. The reduced surface ductility in humid air is attributed to the tangling of dislocations underneath the surface oxide.

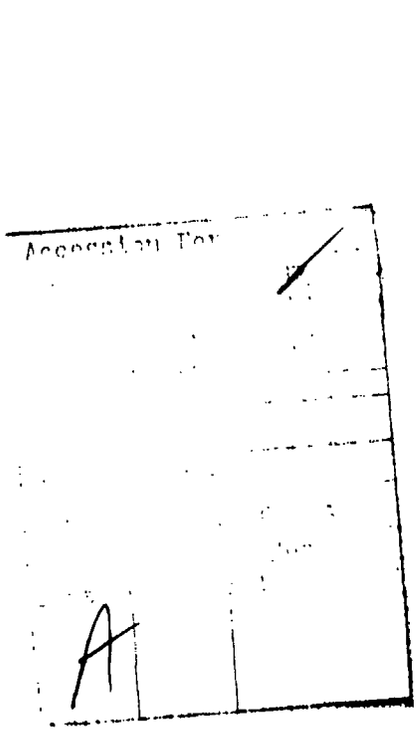

TABLE OF CONTENTS

LIST OF ILLUSTRATIONS

LIST OF ILLUSTRATIONS

LIST OF ILLUSTRATIONS

LIST OF ILLUSTRATIONS

LIST OF TABLES

ABSTRACT

The effects of atmospheric humidity and of internal hydrogen on localized surface ductility of a Al 2219-T851 alloy have been characterized. A reference gauge technique was used to measure the peak tensile plastic strains which develop during fatigue within individual grains at the surface of the alloy. These are senstive to environment and can exceed 0.5%, even when the bulk deformation is linearly elastic. The average strain at the surface is controlled by the subsurface, resulting in a mixed pattern of tensile and compressive strains from grain to grain. The hysteresis loops open more rapidly with fatigue within grains having large distances of slip between boundaries at the surface. Constituent particles are fractured when the width of the local stress-strain hysteresis loop increases to a critical value. A simple strain energy criterion for particle fracture is used to model the probability of particle fracture from the distance of slip from the particle to the grain boundary. Agreement is achieved with experimental data by assuming that environmental factors alter only the local ductility of the matrix material within individual grains, and not the particle fracture surface energy. Ambient humidity is found to decrease the rate of fatigue induced opening of the local stress-strain hysteresis loops. Internal hydrogen increases the rate. Concomitently, substantially more particles are fractured in an alloy containing even small amounts (< 1 ppm) of internal hydrogen.

The local ductility of the surface also plays a role in the rate of propagation of short surface cracks. Crack tip plasticity is much larger than the strains involved in crack initiation, and the sensitivity to environment is partially reversed for crack growth. By measuring crack tip opening displacements we find that both internal hydrogen and ambient humidity reduce the ductility of the material at the tip of small surface cracks. This leads to accelerated growth rates. It appears that at small strains (< 0.3%) hydrogen increases the local ductility of the 2219 matrix material, whereas at large strains (> 1%) it decreases ductility. The observation that humidity and

internal hydrogen change the ductility in opposite directions at small strains provides indirect evidence that hydrogen does not penetrate the oxide surface barrier until a crack is formed. The reduced surface ductility in humid air is attributed to the tangling of dislocations underneath the surface oxide.

1.0 INTRODUCTION

Ambient environment can alter the mechanical properties of metals. Most alloys are susceptible to aggressive environments which corrode the surface or otherwise alter local microstructure and enhance crack initiation and growth. The acceleration of grain boundary cracking due to oxidation of metals at elevated temperature is one of many such effects. In materials embrittled by hydrogen, protons may penetrate below the surface and change bulk properties [1,2]. The modification of alloy elastic modulus by hydrogen is an especially well docomented effect of this type [3]. Some milder environmental-surface interactions apparently result from an interrelationship between surface films and near surface dislocation structure [4]. Usually these effect only the surface, but Duquette [5] has reported one example in which bulk tensile strength is thought to be controlled by non-aggressive surface environments. Cyclic loading apparently enhances environmental effects, probably because the changes are accumulative. Quantitative characterization of the mechanical properties of thin surface layers, subject to environmental influence, has been hampered by the lack of suitable experimental techniques.

We describe here several new methods to measure the small localized plastic surface strains which are precursors to fatigue induced crack initiation and early growth in alloys. One of these [6] allows data to be obtained for alloy matrix material within individual surface grains, so that correlations between environment, local grain size and local microplastic deformation can be studied. These methods are applied to investigate the roles of ambient humidity and of internal hydrogen in determining the ductility of the surface of aluminum alloys.

Two degrees of surface plastic strain are distinguished in assessing the role of hydrogen and humidity on surface ductility.

Small Strain Case - During cyclic linear elastic loading of bulk aluminum specimens, the surface undergoes progressive changes in its

mechanical properties. These changes occur only in grains of appropriate orientation and cross section at the surface and are effected by environment in a pronounced way. The changes are best characterized by measuring the local stress-strain hysteresis loops within individual surface grains. One experimental technique we describe is used to measure a parameter which is approximately proportional to the width of the hysteresis loop.

Large Strain Case - Early growth of short surface cracks involves large amounts of localized plastic deformation at the surface crack tips. By measuring the opening of the crack tip at the surface we obtain a parameter which depends upon the ductility of the material in the plastic zone. This analysis is possible because the size of the plastic zone is constrained by the grain boundaries.

Results from prior years are summarized, and new findings to complete the description of our current understanding of the interplay between environment, local surface ductility, and crack initiation and short crack growth are presented in this report. A strain energy density model of crack initiation at constituent particles is proposed and is used to predict the effect of humidity and of internal hydrogen on crack initiation in Al 2219-T851 from localized matrix microplasticity data. Measurements to assess the relationship of surface ductility to early crack growth during fatigue are also discussed. To conclude, crack initiation and growth models are combined to predict from alloy grain size and hydrogen content the statistical scatter in fatigue lifetime of Al 2219-T851. These predictions are tested experimentally.

2.0 LOCALIZED PLASTIC DEFORMATION OF THE SURFACE - THE SMALL STRAIN CASE

All who have studied fatigue crack initiation recognize that the surface is an especially vulnerable site for crack development. Even for bulk elastic loading, visable microscopic distortions of the surface present graphic evidence of localized plastic deformation during fatigue, apparently permitted by the partial absence of bulk constraints on the dislocation motion. Usually the magnitude of the localized plastic strains are unknown. Also competing mechanisms to rationalize environmental affects can be difficult to assess. For instance, constituent particle fracture in Al 2219-T851 is enhanced by increased alloy hydrogen content. Is this because hydrogen decreases the particle fracture energy, or does hydrogen increase the fatigue induced localized plastic strains in the alloy matrix? Experiments to resolve this question are discussed, and it is concluded that the latter explanation is correct. Also results are presented that, at small strains, internal hydrogen and increased environmental humidity change the surface ductility in opposite ways. We conclude that hydrogen is not the active element in embrittlement of aluminum by water vapor, at small strains. A reference gauge technique to measure surface plasticity is described. Results obtained with this technique are given in detail. A model to predict the probability of constituent particle fracture from local plastic strain is presented and is applied to predict the effects of internal hydrogen and of ambient humidity on constituent particle fracture in two heats of Al 2219-T851 of 30 and 60 μm grain size. These predictions compare adequately with experimental data.

2.1 Measurement of Localized Strains Using Small Reference Gauges

2.1.1 Introduction

For fatigue at stress amplitudes substantially less than the alloy yield strength, plastic slip near the specimen surface is blocked by the grain boundaries [7,8]. Crack initiation is attributable to a progressive increase in localized microplasticity within individual grains [9,10]. Models of this

process are commonly divided into two sequential parts. First, the peak tensile plastic strain produced within an individual grain, on each loading cycle, is predicted with an appropriate model of mobile dislocation development. Next, an initiation criterion is employed to relate the probability of crack formation to the type, geometry and mechanical properties of the site of weakness within the grain and to the peak plastic strain of the matrix material within the grain.

Such models can in principle be validated by comparing predicted and measured rates of crack initiation. If disposable model parameters limit the sensitivity of such evaluations, the model describing microplasticity can instead be tested by directly measuring the amount of fatigue induced plastic strain within individual grains. In this section, we describe a technique to make such measurements which has several advantages over other methods used to obtain similar or related data.

In essence, we use a small (~ 20 μm) flake of mica located within a grain of interest as a reference gauge and measure strains in the surface relative to this gauge in a scanning electron microscope (SEM). This method is more accurate for measuring small plastic strains than selected area backscatter electron channeling [11] or stereoimaging [12], which are best suited to measure plastic strains larger than 0.5%. It also avoids the interperative problem encountered with channeling, where one must calibrate the measurement using uniaxially strained specimens. The sensitivity to measure deformation at the surface with a reference gauge appears to be comparable to that obtained by Pangborn et al. [13] with their use of X-ray double crystal diffractometry, but the reference gauge data are obtained directly in terms of local strain and are simpler to relate to current initiation models. The reference gauge method permits crack initiation models to be evaluated by measuring peak strains in preselected grains containing potential initiation sites of interest.

The capabilities and limitations of the technique are described. Results are presented for an Al 2219-T851 alloy for which progressive fatigue

at stress amplitudes below the yield strength produces increasing plastic strain at the surface, with preference for development of the largest plastic strain in the larger grains. Elastic strains in the smaller grains at the surface are shown to be driven into compression during unloading to accommodate these changes.

2.1.2 The Strain Measurement Technique

The strain measurement technique, illustrated in Fig. 1, utilizes as a reference gauge a flat particle of mica lying on the specimen surface within a grain. We measure the distance L between points A and B on the substrate at zero externally applied stress and then load, in the microscope, the surface through a tensile cycle returning to zero applied stress. The new distance L' between A and B is then determined and the residual cyclic strain parallel to the principal stress axis is defined as

$$\varepsilon = \Delta L/L = (L' - L)/L. \qquad (1)$$

The measurement thus determines the width of the stress-strain hysteresis loop at zero external load. If ε is different from zero, local yielding has taken place, although not necessarily within the grain of measurement. ε is the sum of the local plastic strain and the internal elastic strain necessary to accommodate yielding in surrounding grains.

The mica flake provides a reference which substantially increases the accuracy of the measurement of ΔL. High resolution SEM micrographs are obtained which show both the substrate and the mica edge (Fig. 2). Such micrographs taken before and after loading at each point A and B are then observed with a stereoscopic viewer. Small relative displacement in position between the mica and substrate in the before and after loading pairs causes the edge of the mica to appear to lie at a different depth than the substrate. Displacement of the substrate relative to the mica can accurately be determined with a floating point device such as in common use in aerial mapping

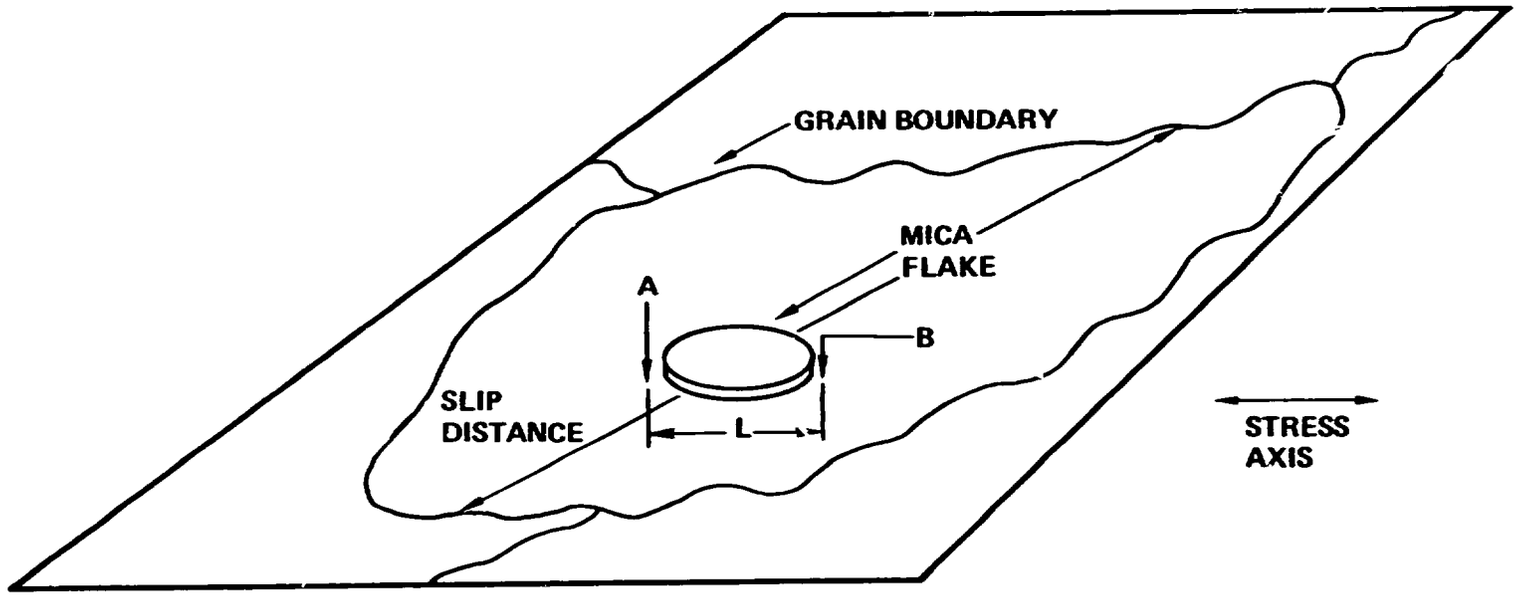

Fig. 1 The reference gauge technique. The mica flake lies within a grain and is not bonded to the substrate. Strain over the gauge length L is determined by measuring the locations of points A and B, before and after loading, relative to the mica. The maximum slip distance D, plotted in Fig. 5, is the larger of the two grain widths through the mica flake, measured at a 45° angle to the principal stress axis.

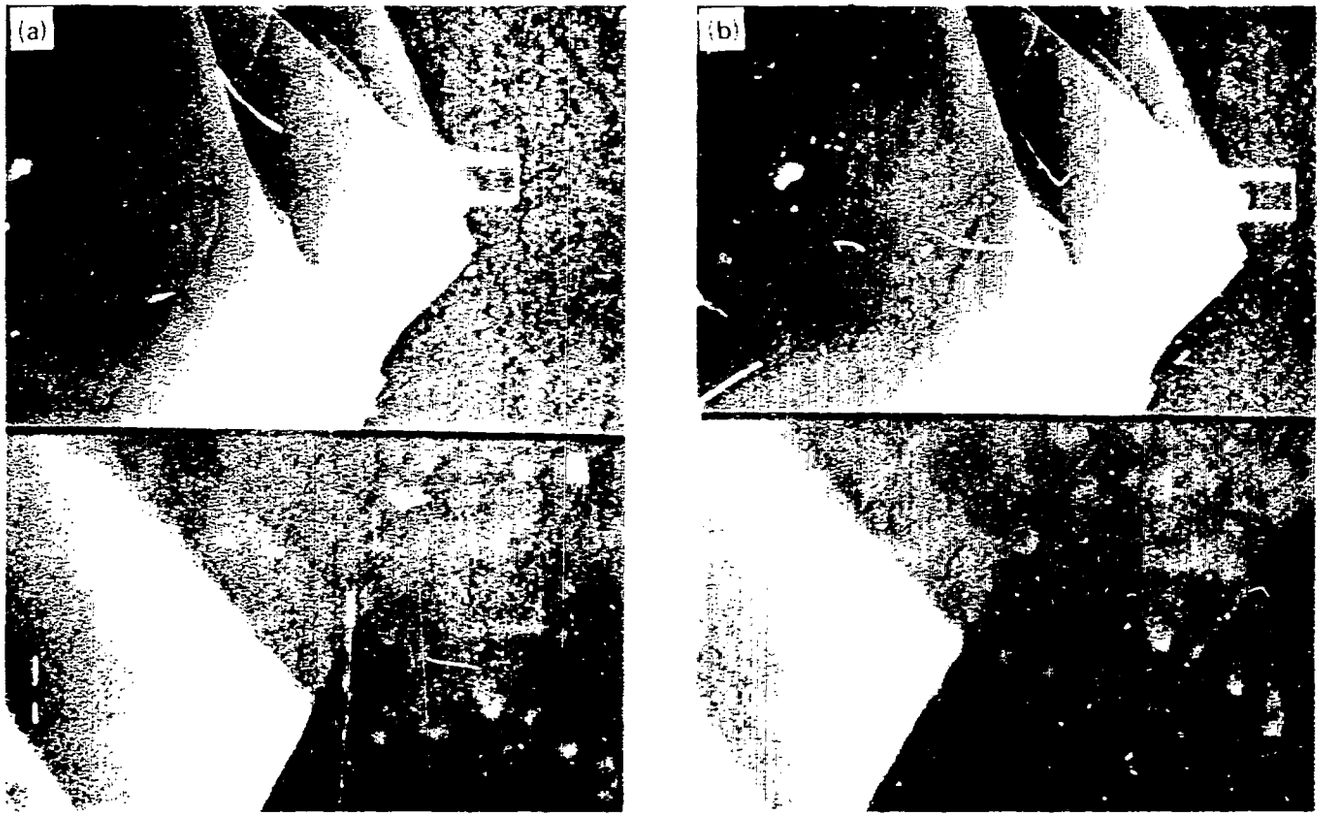

Fig. 2 Typical micrographs of an area near the edge of a mica flake: a) before loading, b) after loading. Dual magnification is used to facilitate relocation of the measurement point after loading with the low magnification half at 3000 X and the high magnification half at 30,000 X. The mica edge is to the left in all views. The substrate in (b) is 580Å further to the right of the mica than in (a). The shift is much easier to see when the pair of micrographs are viewed steroscopically.

(Fig. 3.). The apparent height of the arrow above the substrate is a function of the true distance between the arrows under the viewer. The observer adjusts the traveling arrow so that it first appears to lie at the same depth as the substrate, and then at the same depth as the mica, and records the linear displacement of the traveling arrow by using a micrometer. ΔL is the sum of the linear displacements at points A and B. The human eye uses the entire image to make apparent height decisions and the resulting sensitivity in measurement of displacement can be substantially better than that obtained from direct measurements off the micrographs. With good micrographs the statistical scatter from repeated measurements in displacement obtained with our equipment is $\pm$ 0.005 cm. Using micrographs taken at a magnification of 35×10^3, we can measure ΔL to $\pm$20 Å. The resulting sensitivity in strain is, of course, a function of the gauge length, L. Strains of 0.01% $\pm$0.005 can be measured within individual grains with optimum microscope resolution.

There are several tricks to make this technique work well. Mica flakes in a size range of 15 to 60 μm can be prepared using a rotating blade glass cutter to crush mica in a mortar. The best flakes are very thin and flat so that they maintain close contact with the substrate, and thus both the mica edge and the substrate can be brought into simultaneous focus in the SEM. An added advantage of thin, flat mica flakes is that they are less likely to tilt relative to the substrate as a result of the loading. Such movement would introduce error into the strain measurement. In our experience, tilting occurs for about one particle out of 20 and is easily recognized, since different points on the mica edge appear to lie at different heights. There is no accurate way to correct for tilting and data from such particles are not used. It is not necessary to coat the mica particles to prevent charging in the SEM, but stigmation of the electron beam in the vicinity of a particle measurement site is advisable.

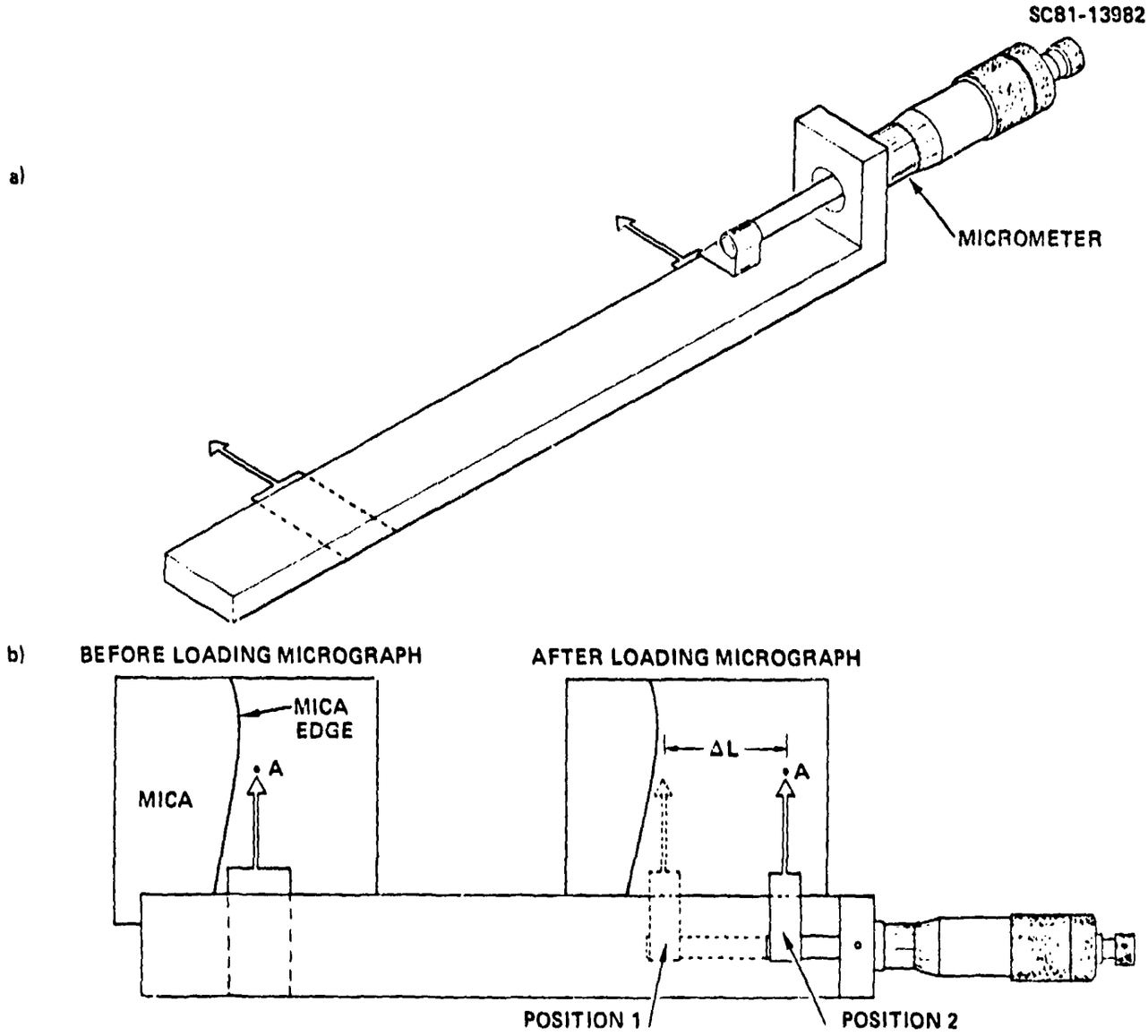

Fig. 3 A floating point device as pictured in (a) is used to measure displacement of the substrate relative to the mica. The pointer on the left is fixed while that on the right moves laterally by turning the micrometer. The observer places the instrument over the two micrographs (before and after loading at the same position, either A or B) and using a stereoscopic viewer, adjusts the traveling pointer so that it first appears to lay at the height of the substrate. This is illustrated in (b) as position 2 (point A on the substrate has moved during the loading cycle). The traveling pointer is then adjusted so that it appears to lie at the same height as the mica (position 1). The linear displacement read on the micrometer is ΔL at point A. Accuracy in the measurement of ΔL is substantially improved by stereoscopic viewing.

2.1.3 Experimental Approach

Tapered cantilever flexural fatigue specimens were prepared from rolled plate stock of Al 2219-T851 with the specimen surface in the rolling plane and with the principal stress axis parallel to the rolling direction. The mean grain size in the rolling direction was 80 μm and in the long transverse direction was 60 μm. The alloy yield strength was 338 MPa. The specimens were machined with progressively decreasing cutting depths to minimize residual surface stresses. They were mechanically polished ending with 0.05 μm Al_2O_3 powder and chemically etched to reveal the grain boundaries. Residual stress measurements using X-ray diffraction indicated all samples were within ±20 MPa of being stress free.

The specimens were fatigued in dry air in flexure, using stroke control and fully reversed loading (R = -1), and were then lightly dusted with mica flakes. Flakes within grains of interest were located by optical microscopy (250x). These were chosen for use as a reference only if they appeared to lie flat on the substrate, with at least 15 μm of gauge length parallel to the stress axis within a grain. A map of the location of each was made using an XY stage on the optical microscope which was then transferred to another map compatible with the XY stage of the SEM. This facilitated the rapid location of the chosen measurement sites in the SEM. The grain size at a measurement site was determined from the optical micrographs.

Flexural loading through the tensile half loading cycle was done in the SEM using the jig pictured in Fig. 4. A reversing drill connected to a rotary feedthrough into the SEM was used to operate the jig. Measurements were made at zero load to avoid tilting of the surface which could introduce error. To obtain the proper hysteresis loop, unloading in air after fatigue was completed through the compressive half cycle.

2.1.4 Example Results and Discussion

Measured values of residual cyclic strain, ε, are given in Fig. 5 for Al 2219-T851, plotted as a function of the maximum slip distance to the grain

SC81-13984

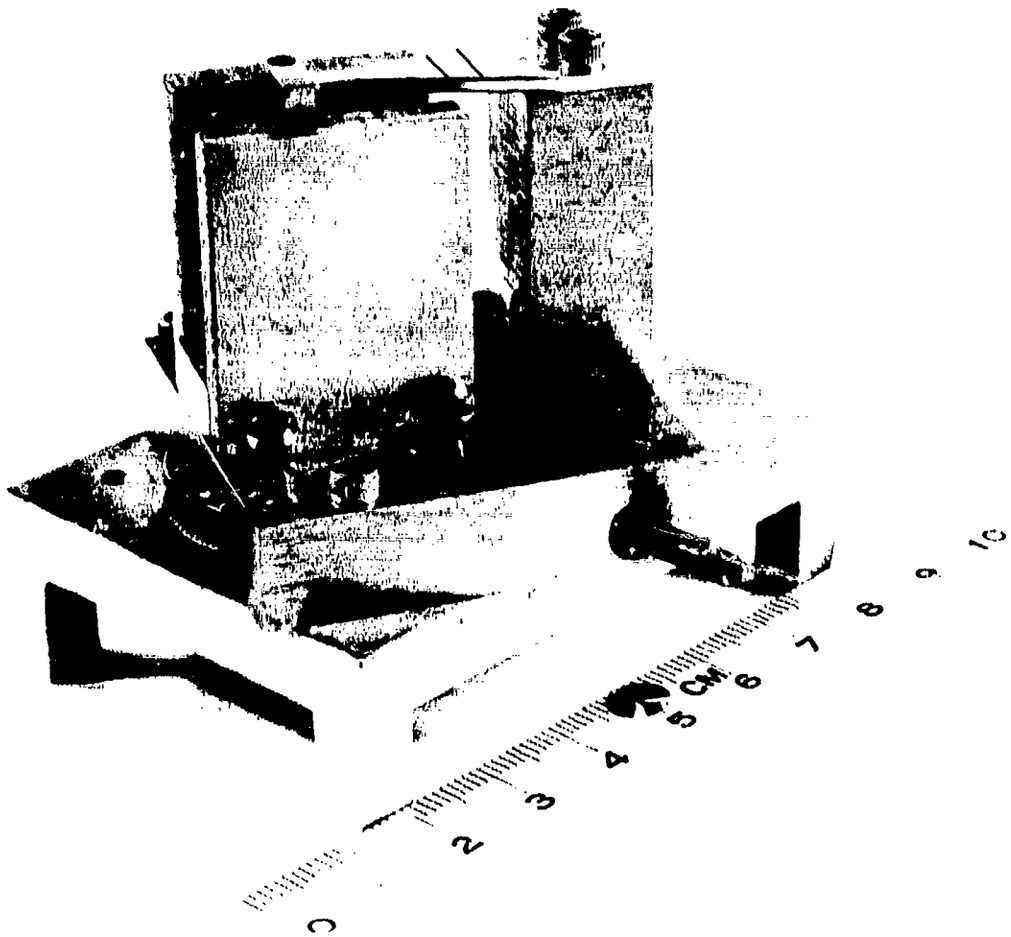

Fig. 4 Jig used to load a flexural fatigue specimen in the SEM. A reversing drill is connected through a rotary feedthrough into the microscope to the shaft A which moves the load bar B up or down along guide shafts via a worm gear. Surface stress on the specimen (C) is calibrated to the deflection of B, which is monitored by counting drill revolutions (typically 450 turns to yield). Data are taken from grains only within the region defined by the parallel lines.

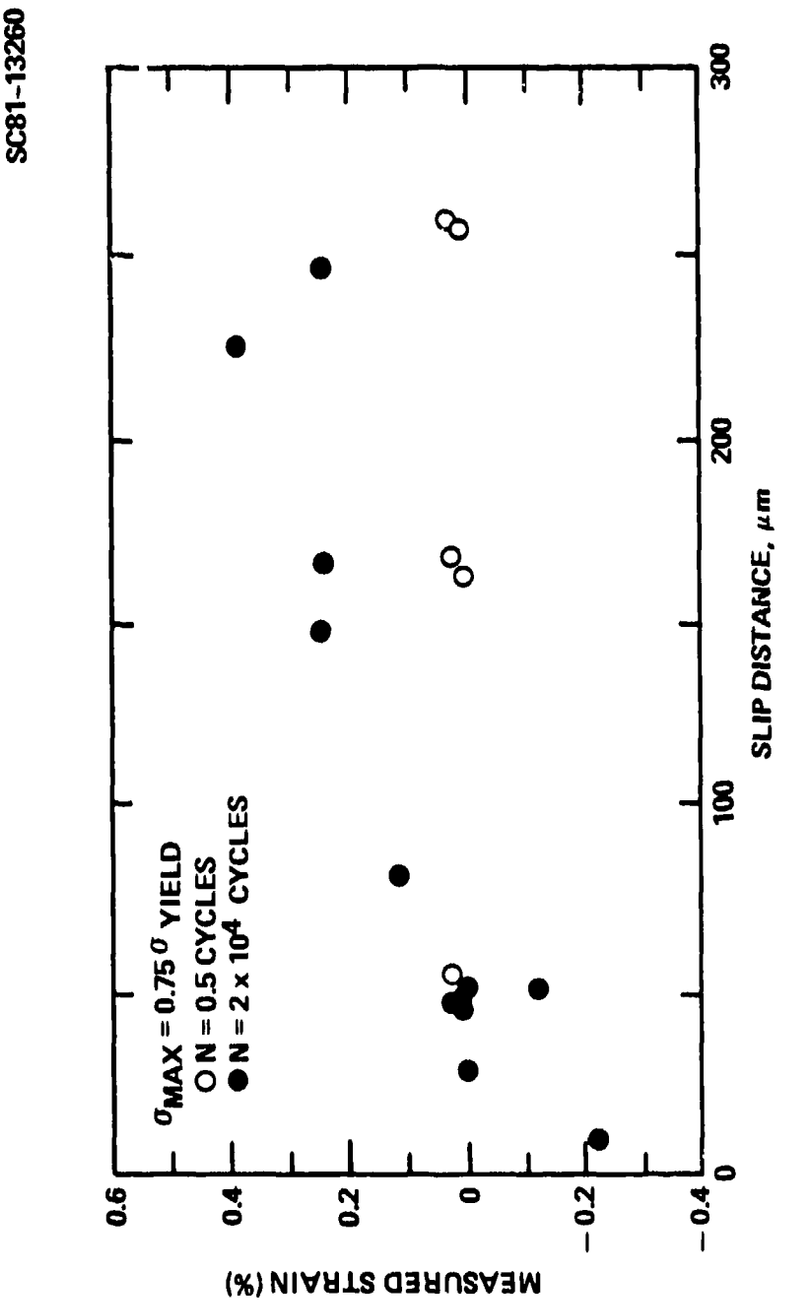

Fig. 5 Measured residual cyclic strain is plotted versus the maximum slip distance through the measurement site for two periods of fatigue.

boundaries measured through the center of the measurement site. As illustrated in Fig. 1, the maximum slip distance within the grain is measured at a 45° angle to the principal stress axis. Data are presented for two cases. The open circles are for a specimen cycled through a single half loading cycle with a peak surface stress of σ_{max} = 270 MPa (0.75 σ_{yield}). The residual strains for all grain sizes are indistinguishable from zero, indicating the material is purely elastic for the first tensile loading cycle.

We have found that, at least initially, values of ε in the larger grains progressively increase with fatigue. Tens of thousands of cycles are required to produce maximum values of ε in the largest grains in the alloy at σ_{max} = 270 MPa. Data after 20 x 10^3 cycles of fatigue in dry air are given by the solid circles in Fig. 5. These clearly show a preference for ε to be largest in the larger grains, consistent with models proposed by Ch: g et al. [14] and Tanaka and Mura [10] describing fatigue crack initiation. The strains are quite large and must require that substantial redistribution of the local stresses within the neighboring grains occur to accommodate the fatigue induced microplasticity. For instance, small grains in which ε is negative are found to lie at the boundaries of large grains in which ε is positive. Apparently, a large grain yields in tension and, on unloading, imposes an elastic compression on itself and neighboring grains. Undoubtably, the true peak tensile plastic strain in the larger grains was larger than the measured ε.

The expected error in the measurement of ε is small compared to the observed scatter, which can be attributed to such factors as the variation of the grain's crystallographic orientation, the depth of the subsurface grain boundary, and the location of the measurement site within the grain. If we allow for a possible 0.2% compressive elastic strain reacting on the large grains, it appears likely that the peak localized tensile plastic strain in the surface may exceed 0.5% after 20 x 10^3 cycles. Thus, it is not surprising that surface constituent particles in Al 2219-T851 fracture in the larger grains in substantial numbers after such fatigue [9,15].

We believe these changes are localized near the surface. No opening of the bulk stress-strain hysteresis loop was observed in axial fatigue of smooth bar specimens of Al 2219-T851 cycled at σ_{max} = 270 MPa, verifying that bulk plastic deformation did not take place. The measurement of residual surface strains thus provides a unique opportunity to study fatigue induced changes in surface ductility, and a comprehensive evaluation of these processes in aluminum and its relationship to crack initiation is presented in Section 2.2.

The possibility of applying the reference gauge technique to measure local modulus and the local flow stress is also apparent. These measurements require determination of strain under load which, on flexural loading samples, causes the surface to tilt. As a result, the measured values of strain will be scattered about the true strain due to a change in perspective of the mica relative to the substrate, as mentioned previously. If the particle is of a nearly uniform thickness, this error will be small. A more direct way to eliminate the perspective problem would be to use an axial loading stage.

2.2 Effects of Ambient Water Vapor and Internal Hydrogen on Surface Microplasticity and Crack Initiation

2.2.1 Introduction

The surface of an alloy is a favorable site for fatigue crack initiation. It is exposed to the ambient environment, and its mechanical properties are altered from those of the bulk by surface oxide and by the partial absence of constraints on the deformation. Pioneering research by Thompson et al. [16] demonstrated that initial fatigue damage can be concentrated very near the surface. They found that periodic removal of shallow surface layers during fatigue extended the fatigue life of commercially pure copper. Kramer [17] has subsequently reported the same effect for a number of materials. But despite many eloquent studies of dislocation structure precursive to fatigue crack initiation, quantitative models of initiation have been slow in developing. Until recently, there has not been a strong need for such insight. Now,

new lifetime prediction techniques require models that predict cycles to crack formation from the localized microstructure at potential sites of crack initiation [18]. A major constraint to the rapid success of recent efforts in initiation modeling has been the extreme difficulty in measuring localized changes in the mechanical properties of the surface which are associated with fatigue. Consequently, there is still no concensus regarding the manner in which fatigue induced deformation in the alloy matrix actually leads to crack formation.

Contemporary theories separate the crack initiation process into two parts. Dislocation models are used to calculate the degree of localized microplastic strains developed within individual grains; the strains are sensitive to local grain size and thus microstructure as well as other ancillary factors such as the environment. The actual cycles to crack initiation are subsequently determined by imposing a fracture criterion which is determined by the nature of the cracking site. For instance, in modeling constituent particle fracture, both Chang et al. [14] and Tanaka and Mura [10] assumed that a particle breaks when the elastic strain energy in the particle equals the energy required to form the new fracture surface. Elastic strain within the particle arises from dislocation pile-ups at the matrix-particle interface. There is ample qualitative evidence, however, that microplasticity is not the only driving force for crack initiation. For example, in Al 2219-T851, the crack initiation habit changes with cyclic stress amplitude as well as with cycles (Fig. 6). Certainly, each fracture mode requires its own initiation criterion. However, all three modes of cracking cannot be responsive to microplasticity alone because their order of occurrence changes with cyclic stress amplitude.

Consequently, the state of deformation of the matrix precursive to crack initiation must be characterized by other factors in addition to its degree of microplasticity. The hardness of the surface appears to be one such factor. Fifteen years ago, Grosskreutz [4] examined near surface dislocation structures in Al 1100 and found them to be sensitive to the mechanical

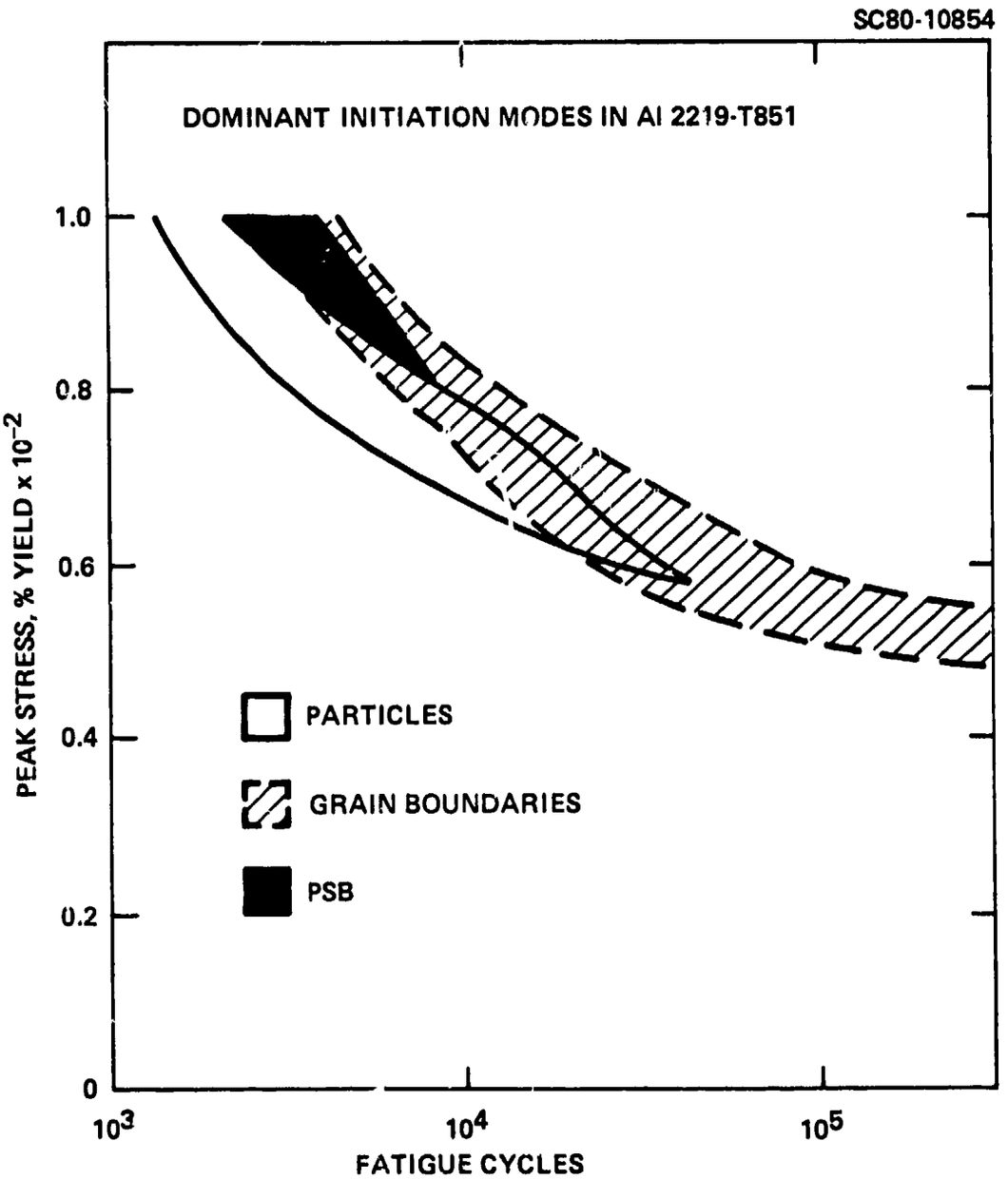

Fig. 6 Multiple microcrack initiation modes are active in Al 2219-T851 and are dominant at different cyclic stress amplitude regimes which tend to overlap as illustrated here.

properties of the surface oxide. Dislocation tangles indicative of hardening in strained samples were more easily developed under the thick coherent oxides which formed in humid air. Subsequently, Kramer [17] has argued that hardening of the surface is required for fatigue crack initiation. Supporting this, Pangborn et al. [13] have recently presented data for an Al 2024-T3 alloy that shows a correlation between localized hardening and fatigue lifetime. Their x-ray double-crystal diffractometry technique involving high resolution imaging of the lattice distortion is biased toward determination of the excess dislocation density in the largest surface grains. It appears, then, that cyclic hardening of the matrix material within a large grain in 2024 may be a precursor to cracking in the grain.

We examine the influence on crack initiation of both localized microplasticity and cyclic surface hardening by measuring local plastic strains within individual grains. Effects of humidity and heat-to-heat variations in the alloy hydrogen content are also assessed by this method. The microplastic response of the alloy surface is characterized by using the reference gauge technique described in Section 2.1. Measurements on Al 2219-T851 show that the localized plastic strains which occur at peak tensile loads within individual grains increase progressively with fatigue at a rate which increases with grain size. While the microplasticity initially increases more rapidly within large grains, its development is ultimately retarded by cyclic hardening of the surface. Furthermore, the maximum microplastic strains obtained during fatigue are effected both by the atmospheric humidity and by the internal hydrogen content of the alloy. Crack initiation in the 2219 alloy takes place at constituent particles, apparently at a critical value of local plastic strain, and thus the rate of particle fracture is sensitive to both humidity and to alloy hydrogen content.

We show that internal hydrogen substantially increases the early development of microplasticity and enhances the rate of particle fracture. Heat-to-heat variations in hydrogen content as small as 1 ppm have an important effect on the fatigue lifetime of Al 2219-T851. Moist air, however, has

an opposite effect in that the development of microplasticity is delayed and the maximum plastic strain is decreased from that attained in dry air. Apparently, the principal effect of humidity on crack initiation in 2219 does not arise from hydrogen liberated by oxidization.

2.2.2 Experimental Procedures

Both crack initiation and localized microplasticity data were obtained with flexural fatigue specimens such as shown mounted in a loading jig in Fig. 4. Specimens were machined from plate stock with the principal stress axis parallel to the rolling direction. The mechanical properties and grain size of each heat studied are given in Table 1. To minimize residual surface stresses developed during machining, each specimen was milled with decreasing cutting depths and then mechanically polished with 0.05 μm Al_2O_3 powder to a mirror finish. Results are given for specimens fatigued in stroke control in fully reversed loading in either dry air or laboratory air at 50-60% relative humidity. The numbers of cracks initiated by fatigue were determined by scanning electron microscopy (SEM), by using the jig in Fig. 4 to place the surface in tension and open the cracks for improved visibility.

Microplasticity and Cyclic Hardening Measurements

Localized microplastic strains were measured by a reference gauge technique that has been fully described elsewhere [6] and in Section 2.1. Briefly, however, the measurements were done as follows. The specimens were lightly chemically etched (etchant of 1.5% HCl, 2.5% HNO_3, 0.5% HF, bal. H_2O) prior to fatigue to reveal the grain boundaries. Fatigue cycling in the ambient environment was completed in compression so that localized plastic strains could be measured over the next tensile loading cycle. Prior to transfer of a specimen into the SEM, small flat mica flakes of approximately 20 μm diameter were sprinkled on its surface. These acted as reference gauges against which displacements in the surface were measured. Micrographs of the location of the substrate relative to the edge of each side of the mica particle were obtained at a magnification of 30,000. The specimen was then loaded in tension in the microscope

Table 1
Material Properties

Chemical Composition*	Heat II	Heat III
Silicon	0.05%	0.07%
Iron	0.22	0.24
Copper	6.02	5.94
Manganese	0.29	0.31
Magnesium	0.008	<0.001
Zinc	0.04	0.03
Titanium	0.07	0.04
Vanadium	0.13	0.11
Zirconium	0.18	0.15
Oxygen	0.0031	0.0024
Nitrogen	0.003	0.001
Hydrogen	High**	Low**
Grain Size		
Longitudinal	45 μm	80 μm
Transverse	30 μm	60 μm
Yield Strength	358 MPa	358 MPa

* Data from Luvak, Inc., Boylston, MA
** All less than 1 ppm. Ranking by bubble densities.

and returned to zero load. A net change in length of the substrate relative to the particle indicates that the surface has yielded microscopically within the vicinity of the particle. New micrographs were taken at the old locations and a stereoscopic technique was employed to measure the displacements of the substrate relative to the mica. These data were then used to calculate the local strain in the substrate over a gauge length which is the width of the mica flake. The procedure measures a residual strain ($\Delta\varepsilon_r$) which is a sum of the tensile plastic deformation and a compressive elastic reaction (due to the constraints from the surrounding grains), with an accuracy of ± 0.005%.

Because of the small size of the mica reference gauges, these measurements can be made within individual grains. Cracking densities were typically low and the measurements were carried out in grains that did not contain fractured particles or microcracks. This alleviated problems that could arise from local compliance changes.

Hydrogen Content Measurements

Heat-to-heat variations in the fatigue behavior of aluminum alloys are common. These are apparently in response to factors such as alloy grain size, and to small fluctuations in composition within the normal range. It appears that small amounts of hydrogen at the 1 ppm level can substantially effect the ductility of the matrix of aluminum. The reference gauge technique allows the true ductility of the alloy matrix to be measured at the surface. We have found two heats of Al 2219-T851 which differ markedly in crack initiation behavior. Gas extraction analysis shows that the hydrogen contents of these are both less than 1 ppm (see Table 1). The relative hydrogen contents of these two materials have been ranked as low (Heat III) and high (Heat II), based on counting of the number of gas bubbles (see Fig. 7) formed in the materials after 3 hours of annealing at 515°C. A histogram of numbers vs bubble diameter is given for the two materials in Fig. 8; this was obtained by sectioning and polishing 0.15 cm thick slabs of the alloys after the annealing procedure.

Further evidence that hydrogen is the active element causing the difference in fatigue behavior between the two materials was obtained by measuring microplastic behavior for hydrogen charged Heat III samples. Charging was done in a salt bath using a modified form of the procedure developed by Elkholy et al. [19]. The apparatus is illustrated in Fig. 9. The salt consists of $NaHSO_4$, $KHSO_4$ and Na_2SO_4 in the proportions 37.5/42.5/160 by weight. Sufficient water was added to produce a melting temperature of 150°C. Charging was done for 4 hours at a current of 200 ma/cm^2. Best results were obtained if no additional water was added during charging. When this

SC81-14401

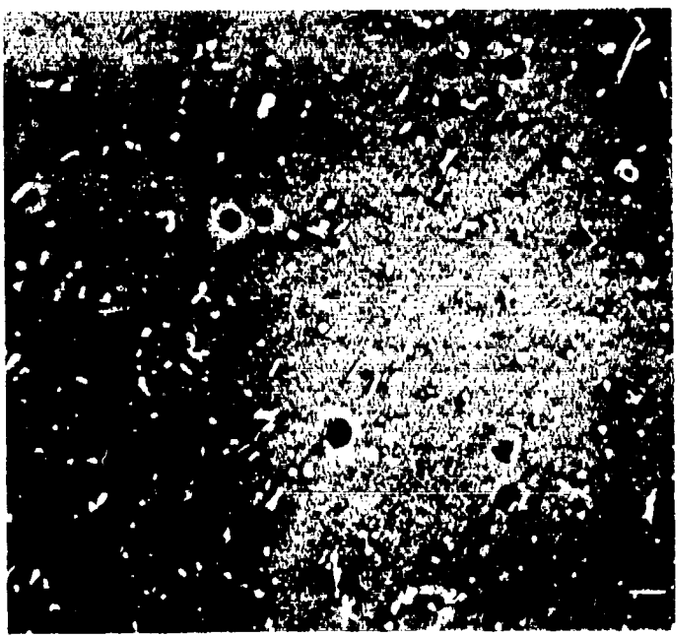

Fig. 7 Scanning electron micrograph of voids at constituent particle sites in Heat II. These are typically hemispherical, suggestive of bubbles. Bar is 10 μm.

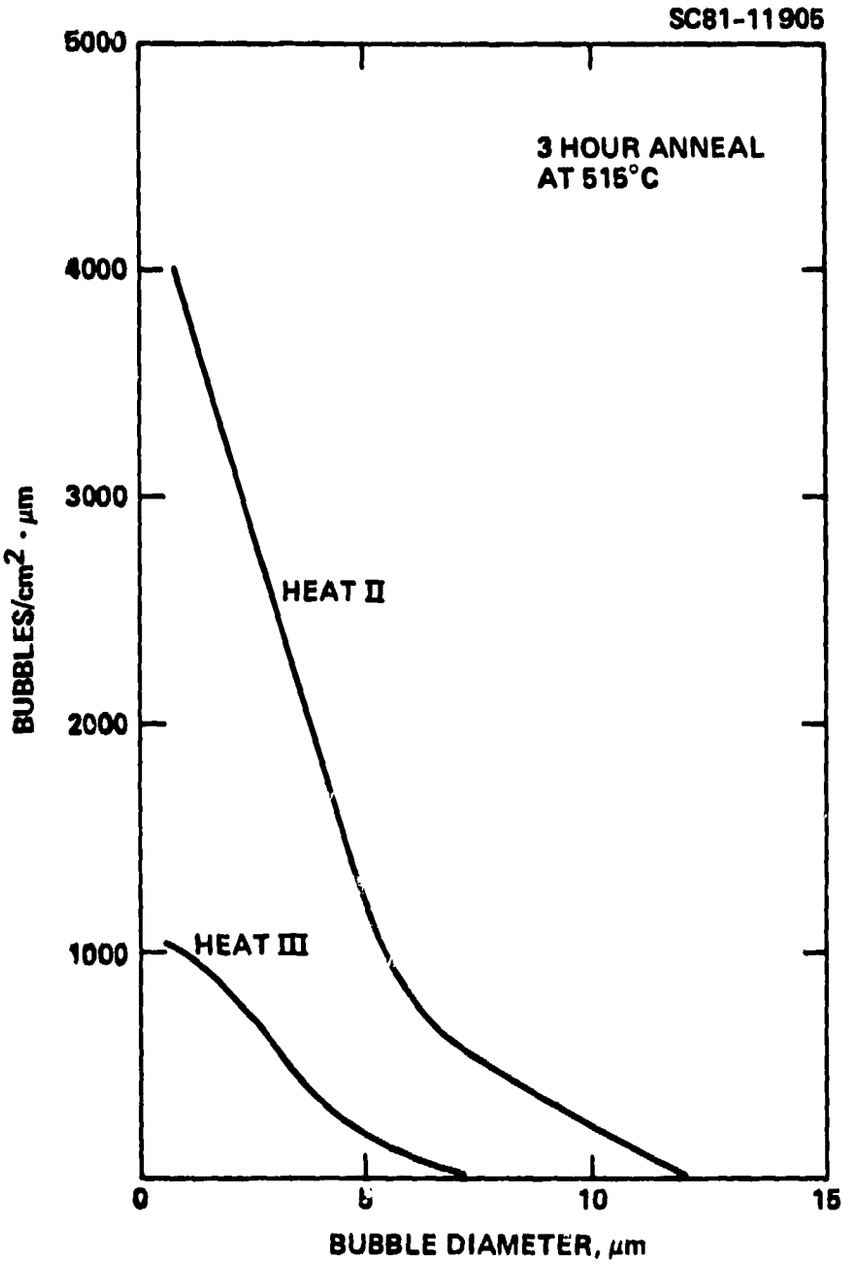

Fig. 8 Histogram of the diameter of bubbles sectioned at the surface of specimens taken from the center of the plate stock for Heats II and III. Specimens were annealed for 3 hours at 515°C.

SC81-14399

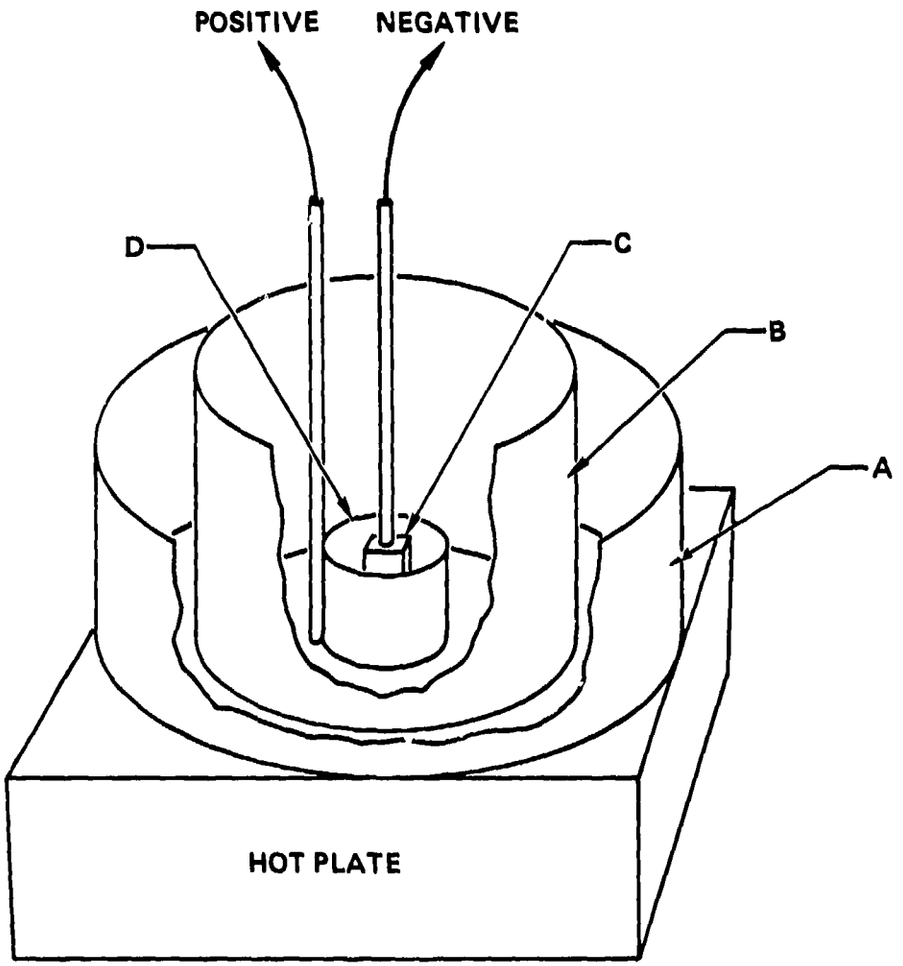

Fig. 9 Schematic drawing of the salt bath apparatus used for hydrogen charging: (a) outer quartz beaker containing diffusion pump oil, (b) inner quartz beaker containing salt, (c) specimen, (d) platinum anode. Although not shown, the charging beaker is also covered by a watch glass.

technique is successfully employed, the specimen surface is not corrosively attacked. Massive amounts of hydrogen are clearly driven into the material, as seen by subsequently annealing the specimens. Grains are actually lifted out of the surface by gas formed at the boundaries (Fig. 10). A redish oxide on the specimen surface is a sure sign that something has gone wrong during charging, and typically results if water is added and not completely mixed with the salt before it contacts the specimen. Specimens exposed to the salt, but not in the charging loop, show no significant change in microplasticity behavior from the uncharged material.

2.2.3 Results

The deformation which leads to the fracture of constituent particles in Al 2219-T851 apparently takes place in a shallow layer near the surface. Particles tend to be more readily fractured in grains having a large surface cross section. Also, polishing to remove only a few microns of the surface noticeably alters the state of cyclic hardening of the material and effects early crack growth. Consequently, we have sought a correlation between $\Delta\varepsilon_p$ (measured on the surface) and grain size, to establish the effect of slip distance on the development of microplasticity. Data are presented for the low hydrogen content Heat III in moist and in dry air, and for hydrogen charged Heat III and Heat II in moist air. The latter material apparently has a high as-received hydrogen content. The development of localized microplasticity is found to be very sensitive to environmental humidity and internal hydrogen. These factors also alter the propensity for particle fracture during fatigue as shown by experimentally determined fractured particle densities. We conclude by demonstrating that measured number of particles fractured by fatigue can be related to $\Delta\varepsilon_p$ using a simple model.

Microplasticity Results

A correlation is sought between measured values of $\Delta\varepsilon_p$ and the size of the grain containing the measurement site. The size parameter evaluated is

SC81-14400

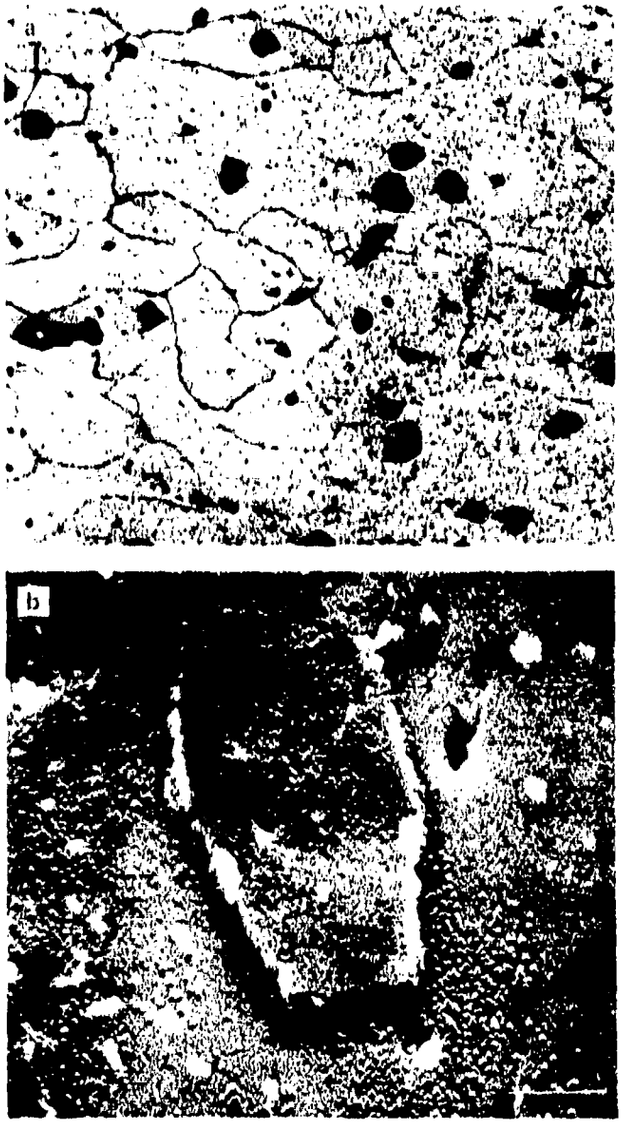

Fig. 10 Micrographs of the surface of a Heat III specimen after hydrogen charging and a 3 hour anneal at 515°C, showing damage to grain boundaries; (a) optical photograph at 250X, the pits are at the sites of constituent particles etched out during charging; (b) scanning electron micrograph showing lifting of a grain out of the surface (bar is 10 μm).

the maximum grain width, D, measured at ± 45° to the principal stress axis; these are the directions of slip presumed most likely responsible for the observed microplasticity, if indeed the deformation is concentrated near the surface. All results were obtained for loading at a cyclic stress amplitude of ± 270 MPa, or at nominally 75% of the yield strength.

Results in Figs. 11 and 12 are from Ref. 15 and are for Heat III cycled in 50% relative humidity air. On the first loading cycle the strain is elastic. With increasing fatigue, plastic strains develop more rapidly at sites of large slip. Curves have been drawn in Fig. 11 and represent expected trends in $\Delta\varepsilon_r$. The strain measurement accuracy is better than ±0.005% strain, as attested by the results at zero fatigue cycles. The scatter in values of $\Delta\varepsilon_r$ is real and probably arises from variations in grain crystallographic orientation and depth. $\Delta\varepsilon_r$ also depends on the properties of other grains near each measurement site. Small grains in which $\Delta\varepsilon_r$ is compressive are found to lie near large grains in which $\Delta\varepsilon_r$ is tensile. Apparently, the small grains are driven into elastic compression in response to residual tensile plastic deformation within the large grains. Thus $\Delta\varepsilon_r$ places a lower bound on the maximum values of microplastic strain, $\Delta\varepsilon_p$, experienced under peak tensile load.

With increasing fatigue, $\Delta\varepsilon_r$ reaches a peak value and begins to fall as the surface continues to cyclically harden. This happens earlier for sites with large values of D. Because of the statistical scatter in values of $\Delta\varepsilon_r$, this behavior is not conclusively demonstrated by Fig. 11. In Fig. 12 results are shown of an experiment in which mica particles were retained at the same locations for measurements after both 5×10^3 and 20×10^3 cycles. It can be seen that $\Delta\varepsilon_r$ has begun to decrease in the 400 μm grains after 20×10^3 cycles, but is continuing to increase in 200 μm grains.

Atmospheric humidity and internal hydrogen both have striking effects on the development of localized microplasticity with fatigue. Samples of Heat III cycled in dry air (~ 0% relative humidity) have substantially increased peak values of $\Delta\varepsilon_r$ (Fig. 13) at 20×10^3 cycles as compared to the

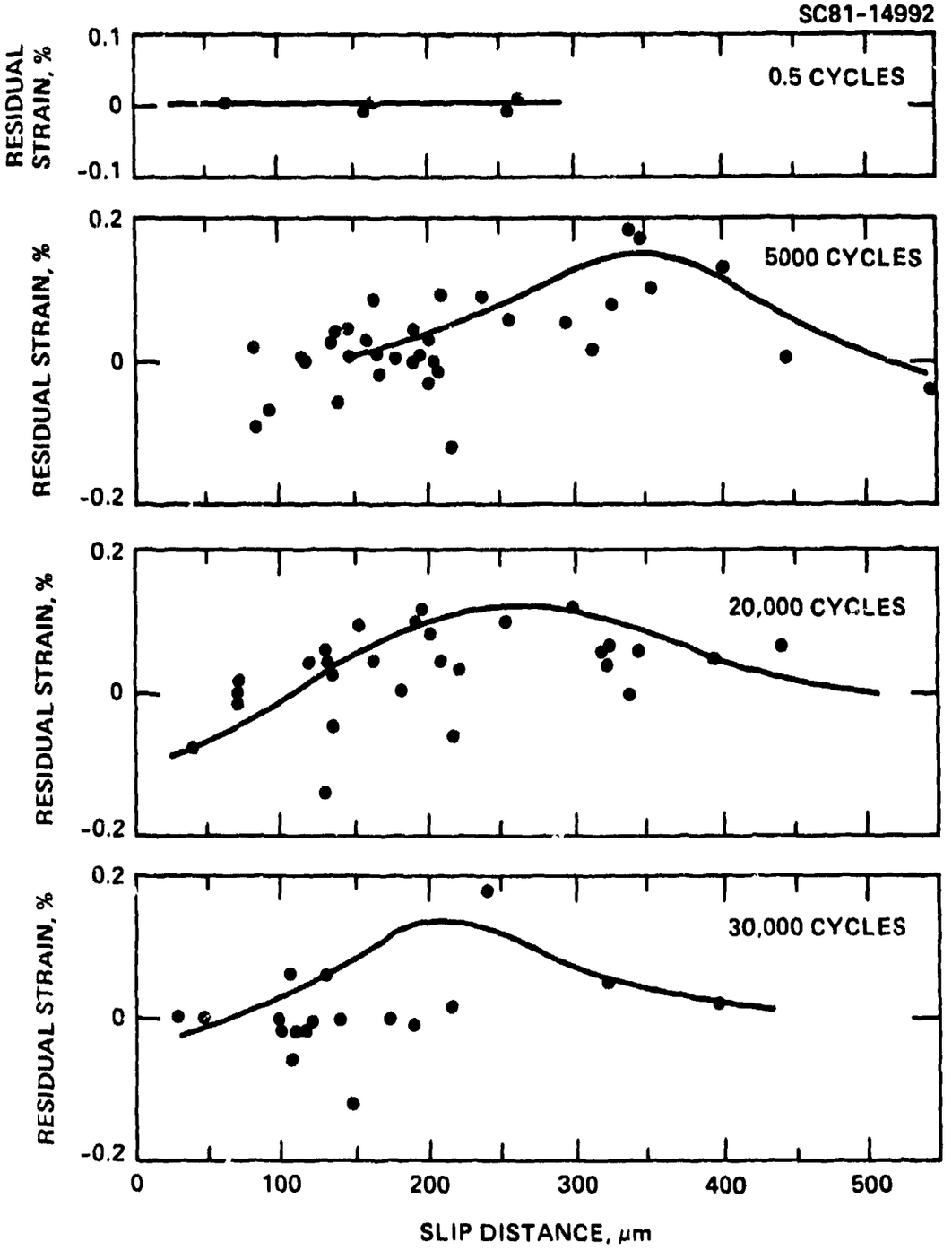

Fig. 11 Residual strain, $\Delta\varepsilon_r$, as a function of slip distance for four intervals of fatigue at a cyclic stress amplitude of ±270 MPa. The solid curves are visual aids that represent expected trends in residual strain.

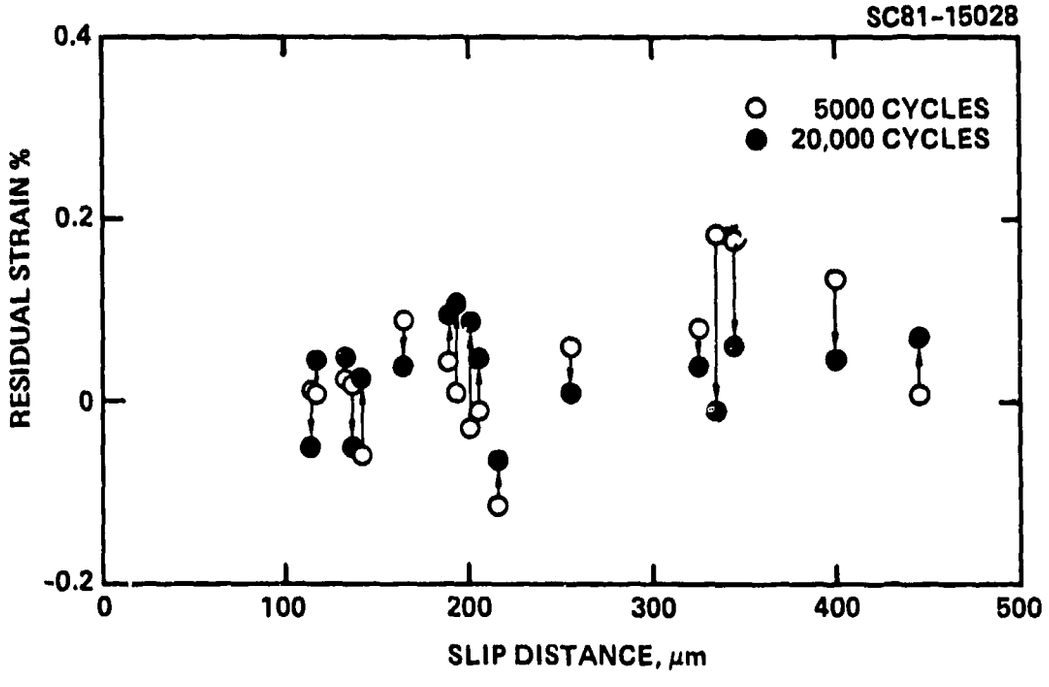

Fig. 12 Trends in development of residual plastic strain are determined by repeated measurements at the same sites. From 5 to 20 × 10^3 cycles hardening has reduced the peak plastic strains in the largest grains, while they continue to increase in 200 μm grains.

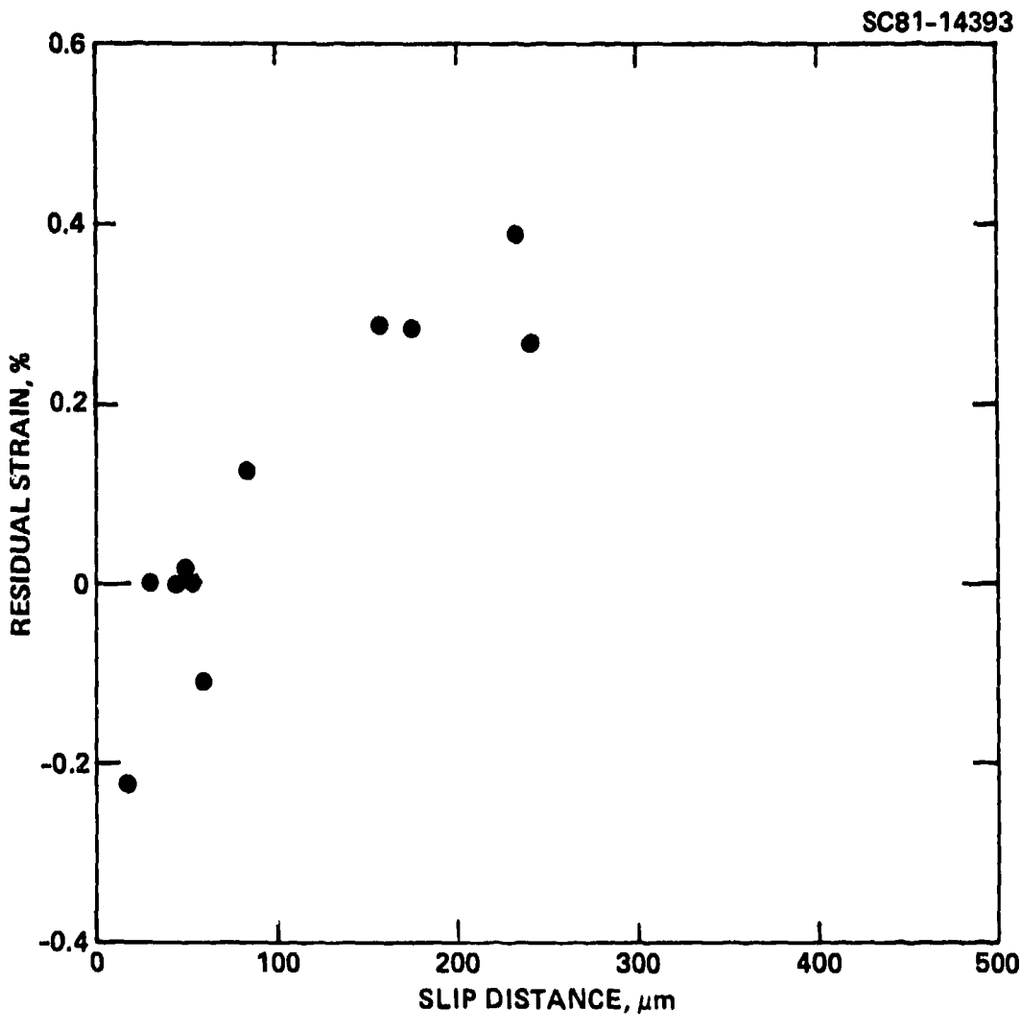

Fig. 13 Measured residual cyclic strain is plotted versus the maximum slip distance through the measurement site for a Heat III sample cycled in dry air for 20×10^3 cycles at ±270 MPa.

50% relative humidity data in Fig. 11. Thus, humidity decreases the peak microplastic strain.

The effect of internal hydrogen content is to increase the initial rate of development of microplasticity for values of $\Delta\varepsilon_r$ up to 0.2-0.3% as seen in Figs. 14 and 15. Thereafter, with additional fatigue, the surface rapidly hardens. The strains in the longer grains become predominantly elastic later during the fatigue lifetime, resulting in $\Delta\varepsilon_r \approx 0$ or $\Delta\varepsilon_r < 0$ if there is tensile plasticity in nearby grains. This effect is quite clear for Heat II material fatigued in 50% relative humidity even though the grain size of this material is only half of that in Heat III (Fig. 14). The data for hydrogen charged Heat III material are in the same direction, but even more pronounced, as seen in Fig. 15. In this case, the sample could only be fatigued to 15,000 cycles before substantial surface cracking developed. All the data at 15,000 cycles exhibited compressive $\Delta\varepsilon_r$ values indicating that only the numerous grains with sizes less than 50 μm were still being plastically deformed. $\Delta\varepsilon_r$ could not be measured in these small grains because the mica flakes invariably lay on a grain boundary.

Fractured Constituent Particle Results

In Al 2219-T851, most constituent particles are β-phase (Cu_2FeAl_7) and range in size from 1 to 25 μm [20]. The particle size distribution for Heats II and III are essentially the same, and are given in Fig. 16. Larger particles tend to fracture first during fatigue [21]. This is apparently a consequence of a critical strain energy criterion for fracture. Also, constituent particles within the large grains tend to fracture first, in response to the more rapid development of microplasticity within those grains [15,21]. The numbers of particles/unit area fractured during fatigue changes with environmental humidity and with internal hydrogen content. More particles are broken in those 2219 materials in which peak values of $\Delta\varepsilon_r$ are large and are reached rapidly. To quantify this observation, counts were made of the numbers of particles fractured during fatigue as a function of their maximum

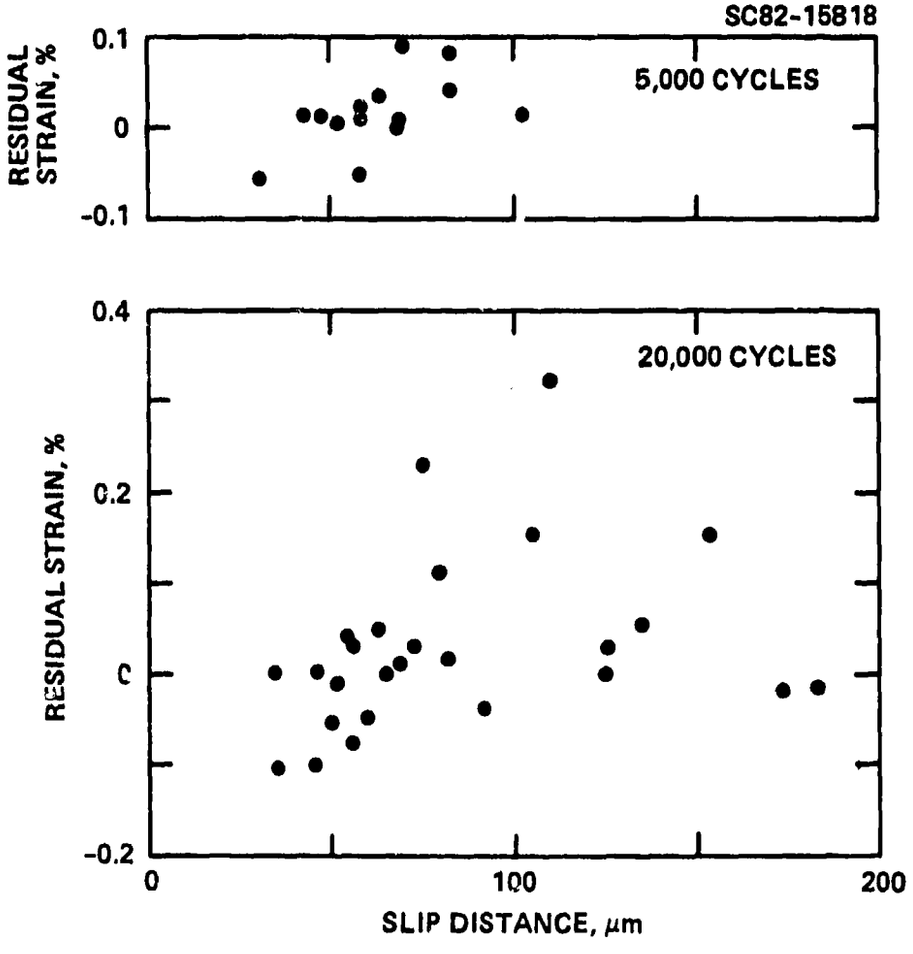

Fig. 14 Measured residual strain vs maximum slip distance for Heat II material which is high in internal hydrogen content.

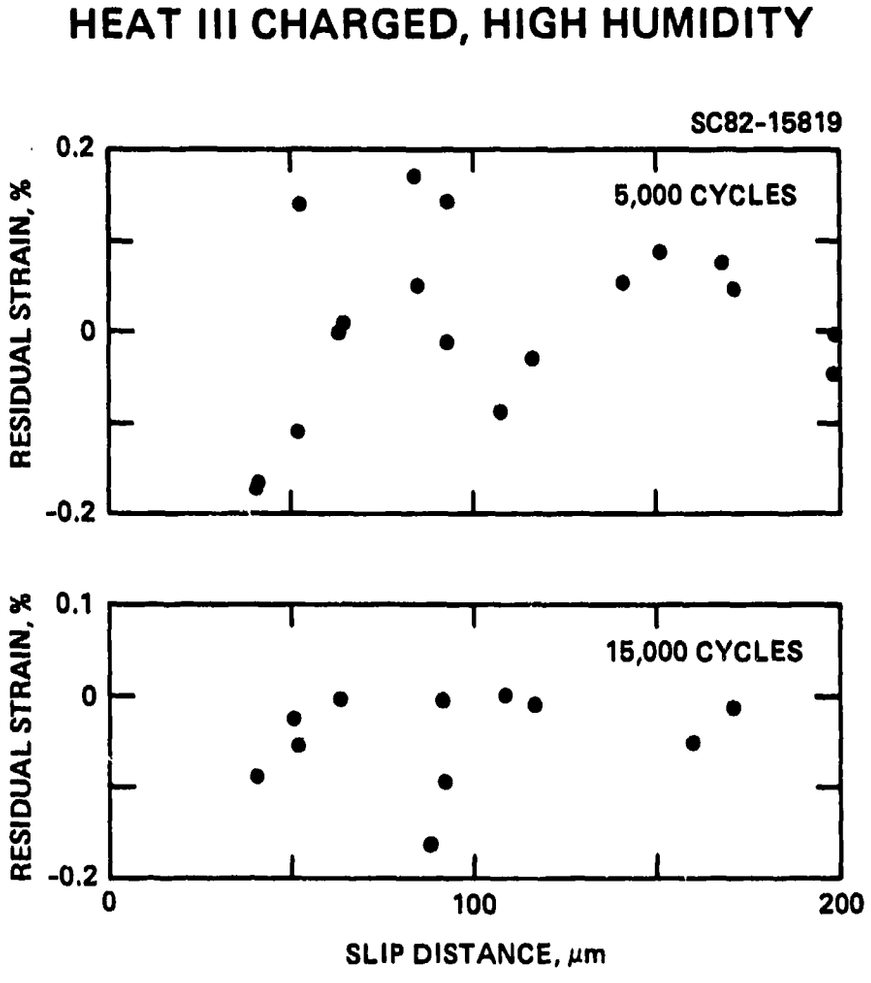

Fig. 15 Measured residual strain versus maximum slip distance for hydrogen charged Al 2219-T851 Heat III material.

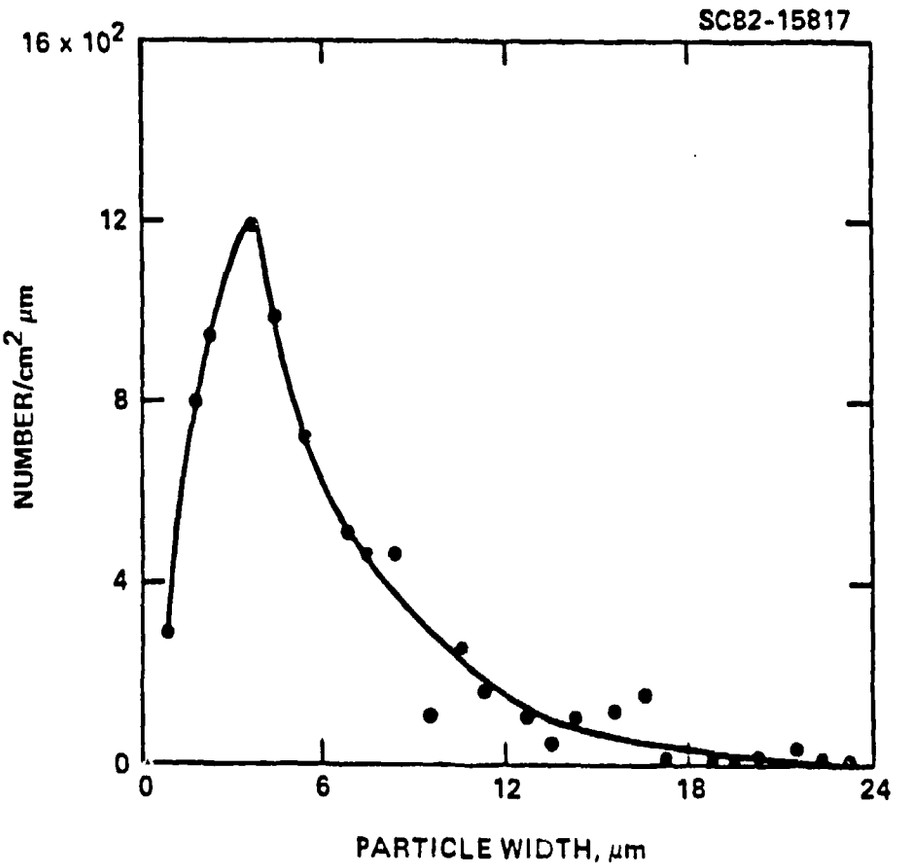

Fig. 16 A histogram of the intermetallic particle width for Heat II and Heat III materials combined. The dimension measured is normal to the applied stress axis, and hence, normal to the rolling direction.

distance of slip (at ±45°) from the grain boundaries. Specimens were fatigued, and both fractured and unbroken particles were located by SEM. Later, the specimens were chemically etched to reveal the grain boundaries so that the ratio of fractured particles to total available particles (> 2 μm) having a given maximum slip distance could be determined. Compared in Fig. 17 are measured and predicted numbers of particles broken (plotted as a probability) versus slip distance for four cases. The cyclic stress amplitude for all experiments was ±270 MPa, the same as used to measure $\Delta\varepsilon_p$. The slip distance D is defined as illustrated in Fig. 18. The curves in Fig. 17 are predicted by the model described below. We have assumed that the environment alters only the surface microplasticity (i.e., $\Delta\varepsilon_p$), not the particle fracture energy, and have calculated the number of fracture events by using the measured values of $\Delta\varepsilon_p$. The statistical errors are especially large for large D because the number of particles having a slip distance more than 150 μm in an individual specimen is small.

Consistent with our microplasticity observations, particles in the larger grains have a greater probability of fracture. Also, comparatively more particles are fractured in those materials containing more hydrogen (i.e., in hydrogen charged Heat III, Fig. 17a, and Heat II, Fig. 17b). The effect of hydrogen in Heat III is so dramatic that it took only 5000 fatigue cycles (Fig. 17a) to fracture more particles than in the uncharged material fatigued for 20×10^3 cycles (Fig. 17d).

Fewer particles are broken for Heat III fatigued in moist air (Fig. 17d) as compared to dry air (Fig. 17c). Given the severe approximation made in the model used in making the predictions shown, the agreement between theory and experiment is good and strongly indicative of the major role of localized plasticity in particle fracture. One anomalous observation is that for Heat III fatigued in moist air, more particles are fractured in small grains than predicted.

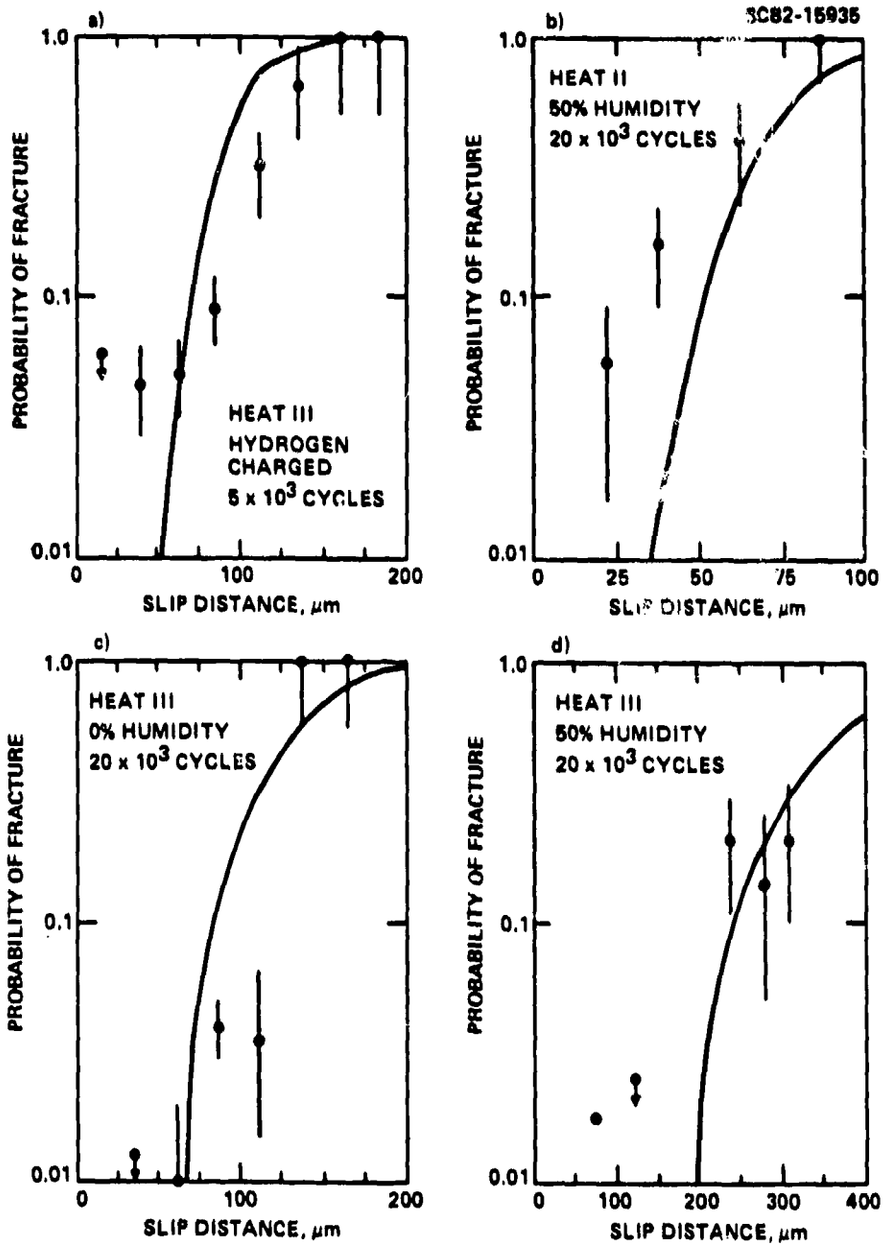

Fig. 17 Probability of a particle being fractured versus slip distance for Al 2219-T851 for both heats. The data are plotted as a histogram over 25 or 50 μm intervals in slip distance. The bars denote statistical measurement error. The solid curves are predicted from the particle fracture model.

SC81-16062

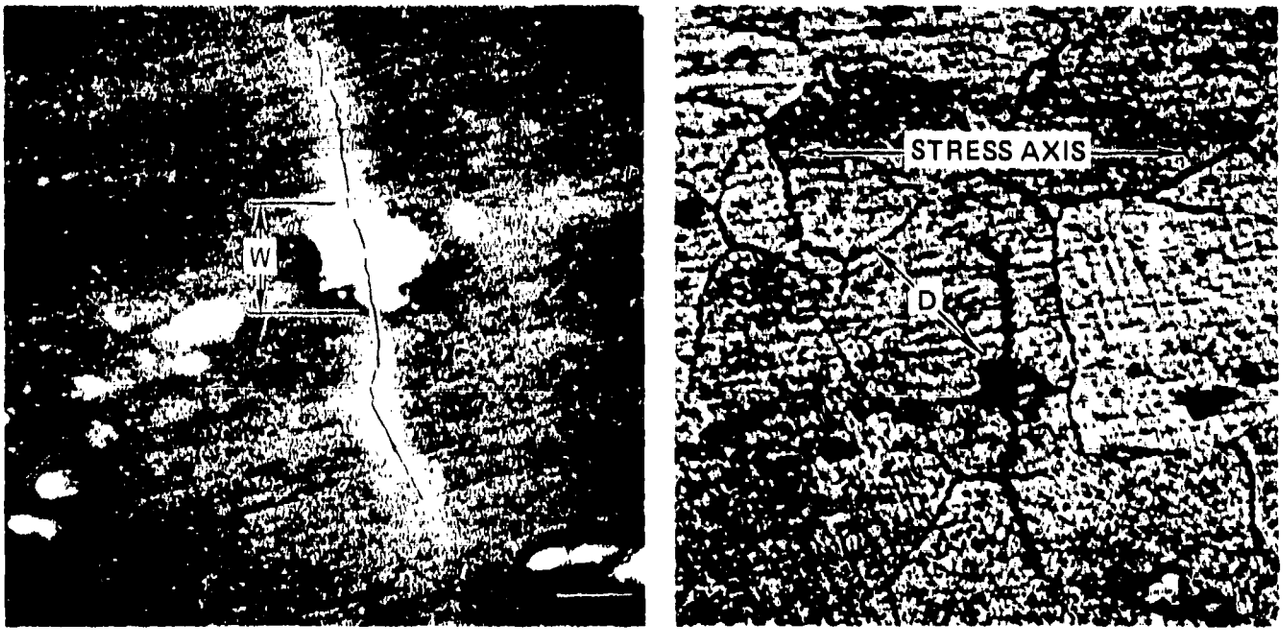

Fig. 18 (a) SEM micrograph of a fractured intermetallic particle. Particle width, w, is measured normal to the stress axis. The bar in the lower left corner represents 10 μm. (b) Optical micrograph illustrating the slip distance, D, as the maximum distance from particle to grain boundary at 45^{0} to the stress axis. The sample has been etched to reveal the grain boundaries after fatigue. The view is normal to the surface.

Particle Fracture Model

We present a model to predict from measured values of $\Delta\varepsilon_r$, the fraction of particles having a maximum slip distance, D, from a grain boundary which will have fractured by N fatigue cycles. We neglect the effect of crystallographic orientation of the grains on $\Delta\varepsilon_r$ and define from experimental values of $\Delta\varepsilon_r$ a parameter $\Delta\varepsilon_{pmax}(N,D)$, which is the maximum plastic strain that occurs in a grain at or before N cycles. An expression is derived to relate $\Delta\varepsilon_{pmax}$ to the size of the smallest particle, w_{min}, having slip distance D which will fracture by N cycles. The percentage of particles fractured is then determined by using the distribution in particle sizes given in Fig. 16, and is simply the number of particles larger than w_{min} divided by the total number of particles. $\Delta\varepsilon_{pmax}$ changes with both alloy hydrogen content and with ambient humidity, and the predicted effect of these parameters on particle fracture, given in Fig. 18, derives entirely from their effect on $\Delta\varepsilon_{pmax}$.

After N cycles, the maximum (upper bound) values of $\Delta\varepsilon_r$, ($\Delta\varepsilon_{rub}$) measured versus D varies as illustrated in Fig. 19. One expects from the models of both Chang et al. [14] and Tanaka and Mura [10] that $\Delta\varepsilon_{rub} \propto D$ for small D. In the data presented here, this trend is partially obscured by the compressive reaction strains. Because of cyclic hardening, $\Delta\varepsilon_{rub}$ illustrated in Fig. 19 is small for large grain size. It is clear from the data in Fig. 11, however, that much earlier during fatigue, $\Delta\varepsilon_r$ was large for large D. $\Delta\varepsilon_{rmax}(N,D)$ is defined to be the maximum values of residual strain experienced at or prior to N cycles, and is illustrated by the dashed line in Fig. 19. We assume that $\Delta\varepsilon_{pmax} \propto \Delta\varepsilon_{rmax}$. For clarity, we have displaced these two quantities in Fig. 19, but because one proportionality constant is used in the model described below, it suffices to set $\Delta\varepsilon_{pmax} = \Delta\varepsilon_{rmax}$. To reiterate, the difference between $\Delta\varepsilon_{pmax}$ and $\Delta\varepsilon_{rmax}$ is that the compressive reaction forces have been added to $\Delta\varepsilon_{rmax}$ to obtain $\Delta\varepsilon_{pmax}$, the actual maximum plastic strain possible in a given grain. Finally, as shown in Fig. 19, a linear approximation is made to give $\Delta\varepsilon_{pmax} = \alpha D$. Parameter α is determined for each of the four combinations of N and material listed in Table 2, by

SC82-15936

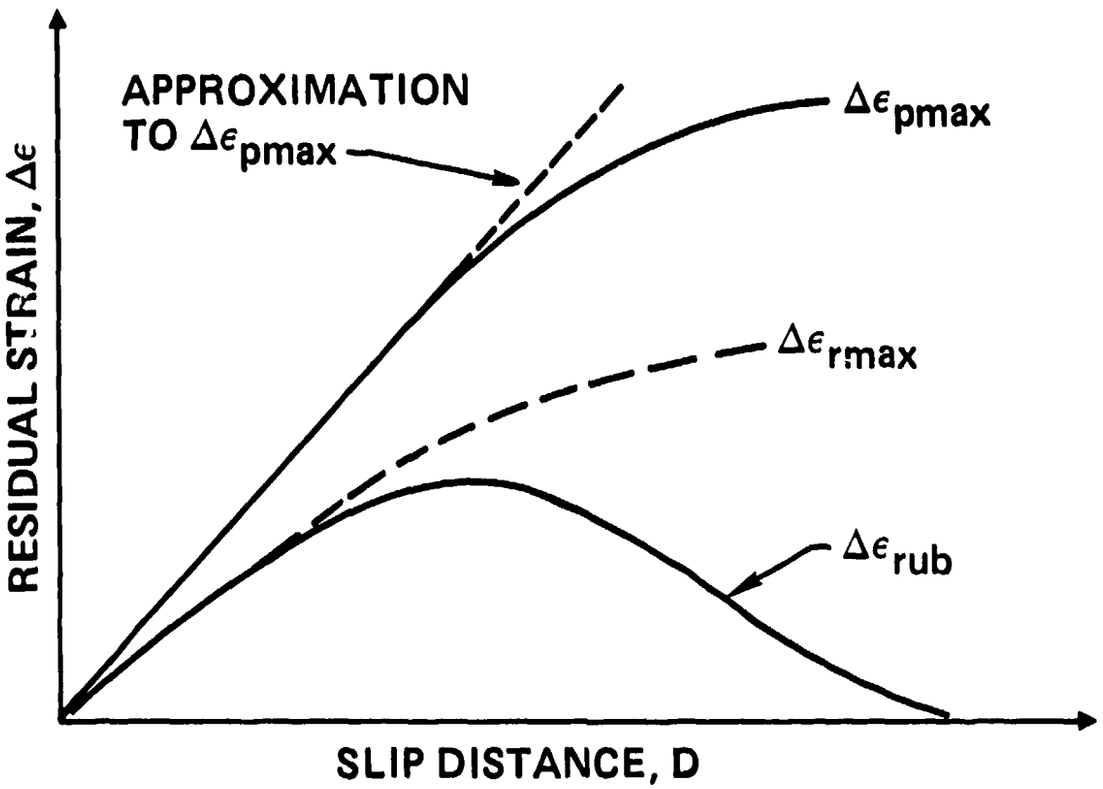

$$\Delta\epsilon_{pmax} = \alpha D$$

$$\alpha = f(N, H, R.H.)$$

Fig. 19 Schematic representation of the change in residual strain, $\Delta\epsilon_r$, as a function of slip distance, with increasing fatigue.

placing an upper bound line of the form $\Delta\varepsilon_{rmax} = \alpha D$ through the experimental microplasticity data given earlier.

Table 2

Approximate Values of $\Delta\varepsilon_{pmax}$ (N, D)

Material	Cycles (N)	$\Delta\varepsilon_{pmax}$ vs D (μm^{-1})
Heat III Hydrogen Charged	5×10^3	2.24×10^{-5} D
Heat III 0% Humidity	20×10^3	1.73×10^{-5} D
Heat III 50% Humidity	20×10^3	0.6×10^{-5} D
Heat II 50% Humidity	20×10^3	2.97×10^{-5} D

A criterion for fracture proposed by Chang et al. [14] is that, at fracture, the stored elastic strain energy within the particle is equal to the energy required to produce the fracture surface. Thus for a perfectly spherical particle

$$\frac{4\pi}{3}\left(\frac{w}{2}\right)^3 \cdot \left(\frac{\Delta\varepsilon_{pmax}}{2}\right)^2 = 2\gamma\left(\frac{w}{2}\right)^2 \qquad (1)$$

where γ is a surface energy/area and w is the width of the particle. We make the approximation that all particles have the same value of γ, and hence, for a given plasticity the smallest particle which will fracture has width

$$w_{min} = \beta/(\Delta\varepsilon_{pmax})^2 \qquad (2)$$

where β is a parameter dependent on γ. A value for β is chosen based on the experimental observation that all particles 2 μm wide and larger are fractured in the hydrogen charged Heat III material for D in the range of 150 to 175 μm. $\Delta\varepsilon_{pmax} = 0.00363$ for D = 162.5 μm in this material, so

$$\beta = 2\ \mu m \cdot (0.00363)^2$$

$$= 2.63 \times 10^{-5}\ \mu m \quad . \tag{3}$$

The predicted fraction of particles having slip distance D which are fractured was calculated for the four cases considered in Fig. 17 by using Eq. (2). $\Delta\varepsilon_{pmax}$ for a given D was extracted from Table 2, and w_{min} was found using $\beta = 2.63 \times 10^{-5}$ μm. Finally, we assumed that all particles larger than w_{min} fractured and determined the resulting fraction of the total available for fracture by integration of the area under the particle size distribution function in Fig. 16.

2.2.4 Discussion

Measurements of surface microplasticity characterize the mechanical properties of the alloy matrix at the surface and provide a unique means to investigate fatigue crack initiation. One might anticipate that hydrogen and environmental humidity would decrease the fracture strength of constituent particles, as well as alter the ductility of the matrix. These possibilities were examined separately by using microplasticy measurements to determine the effect of environment on matrix ductility, and by comparing values of localized plastic strain with the propensity for particles to fracture. With one exception discussed later, we conclude that the substantial effects of environmental humidity and of internal hydrogen on the numbers of particles in Al 2219-T851 fractured during fatigue is due to the changes these factors induce in the ductility of the alloy matrix at the surface.

Internal hydrogen increases the initial rate of formation of localized plasticity within individual surface grains. Humid air decreases the formation of localized plasticity, as compared to that for fatigue in dry air. This trend is valid for small plastic strains in the range of 0.2-0.3%. It is persuasive evidence that the effect of humidity on surface ductility does not arise from hydrogen liberated by oxidation of the surface.

In Table 3, we use the parameter α to rank the four investigated combinations of environment according to their effect on matrix ductility. α is the material parameter in the relationship $\Delta\varepsilon_{pmax}(N) = \alpha D$, and has been extracted by analysis of microplasticity data as discussed earlier. Since $\alpha(N)$ is a function of fatigue cycles, N, only the three combinations for which data were obtained at 20,000 cycles can be compared directly. The fatigue lifetime of hydrogen charged Heat III material was too short to experimentally determine α accurately at 20,000 cycles. A crude estimate suggested by the theory of Chang et al. [14] is that $\alpha(20,000) = 4 \cdot \alpha(5,000)$; this has been used to provide the value listed in Table 3.

Table 3
Effect of Environment on Matrix Ductility

Material	Environment	α (20,000) (μm^{-1})
Heat III Low H	50% R.H.	0.6×10^{-5}
Heat III Low H	0% R.H.	1.73×10^{-5}
Heat II High H	50% R.H.	2.97×10^{-5}
Heat III Hydrogen Charged	50% R.H.	8.96×10^{-5}

Naturally, combinations of materials and environment giving smaller values of α are those which display the least microplasticity, and in which the fewest particles are fractured by fatigue. It appears that hydrogen increases the rate of formation of localized plastic strain in 2219 fatigued in 50% humidity by a factor of 5-15 depending on the alloy hydrogen content. The amounts of hydrogen that lead to these changes are too small to accurately characterize, but for Heat II are known to be less than 1 ppm by weight. One concern was that aging of the 2219 during charging in the hot salt might have contributed to i s change in properties. This appears not to be the case; charging induced only minor surface damage which was removed by polishing prior to fatigue. Also, two specimens exposed to the hot salt but placed outside of the charging loop retained the fatigue lifetime and microplasticity characteristic of uncharged material.

We draw three conclusions from the agreement between predicted and measured numbers of constituent particles fractured by fatigue, shown in Fig. 17. First, at the cyclic stress amplitude used, elastic strain in the particles resulting from localized microplasticity substantially exceeds the elastic strain from the external load, and is the prime factor in particle fracture. Second, the surface energy of the fracture plane is essentially the same for the preponderance of the particles, and is insensitive to either hydrogen content or to humidity. Third, hydrogen and humidity act to induce changes in numbers of particles fractured by altering the propensity of the matrix at the surface to undergo microplastic deformation. Because of the simplistic nature of the model of particle fracture, however, small direct effects of the environment on particle fracture energy would not be unambiguously detectable. Also, not shown in Fig. 17 is an error band around the predicted values that results from the measurement of $\Delta\varepsilon_p$, which further precludes the detection of such small effects.

Actually, quite by accident, we discovered one anomaly which suggests that not all the particles have the same fracture surface energy, γ. In the Heat III material fatigued in 50% humidity, more particles were fractured in 75 μm grains than predicted. We might have been content to ascribe this

difference to the simplicity of our fracture model, but after chemical etching of the surface to expose the grain boundaries for slip distance measurements, we discovered that these fractured particles belong to a subset (<3%) which were heavily attacked by the acid. These probably have a smaller than average γ. Their chemical composition is indistinguishable (as measured by energy dispersive x-ray analysis) from the remainder of the particles. Perhaps their lower fracture energy is related to their structure.

A complete theory of constituent particle fracture by fatigue should include modeling of the development of localized microplasticity and of the cyclic hardening of the surface which limits it. Elsewhere [15] we have discussed the functional form of models which can be used to predict $\Delta\varepsilon_{pmax}$. These were semi-empirical and required material parameters which can be difficult to measure and which we therefore treated as empirical constants. The approach incorporated the effects on particle fracture of grain crystallographic orientation and of cyclic hardening of the surface. Consistent with the new observations above, it was necessary to assume that the constituent particles have a range in γ values to explain the fracture of some small particles at lower cyclic stress amplitudes.

A more fundamental derivation of an expression to predict $\Delta\varepsilon_{pmax}$ is needed. Results reported here on the effect of environment on microplasticity may provide some guidance for this, by indicating the mechanisms which control its development. Because internal hydrogen increases microplasticity at small plastic strains, while humidity decreases microplasticity, we attribute the humidity effect to surface oxide. Grosskreutz [4] has reported that tenacious oxides of aluminum can lead to near-surface tangling of dislocations in monotonically loaded specimens. We believe that the same mechanism is responsible for the small ductility of the surface when fatigued in humid air. Presumably, the oxide inhibits motion of dislocations through the surface. Apparently, at small strains, hydrogen does not cross the surface oxide barrier, and so leaves the material uneffected.

In hydrogen rich 2219, cyclic hardening of the surface is very rapid after $\Delta\varepsilon_p$ exceeds 0.2% to 0.3%. Similar responses of Ni [22] and iron alloys [23,24] to hydrogen in monotonically loaded specimens have been reported, and consist of apparent enhanced ductility at small plastic strains and decreased ductility at large strains.

We report in Section 3.0 that the plastic deformation associated with short surface crack growth in Al 2219-T851 is less in the hydrogen rich material. This is yet another, and the more typically observed, manifestation of the embrittlement of hydrogen at large plastic strains. Thus, it appears that hydrogen degrades the fatigue performance of Al 2219-T851 in two ways. At small strains it enhances microplasticity and accelerates crack initiation. At large strains it reduces ductility and accelerates crack propagation. It is hoped that continued research will ultimately allow these processes to be accurately modeled.

2.3 Localized Surface Hardening at Small Strains

2.3.1 Introduction

Results in Section 2.2 show that with repeated fatigue the stress-strain hysteresis loop within individual surface grains slowly opens from the initially elastic condition. This is apparently in response to a progressive increase in mobile dislocations within the grain. After substantial fatigue the loop closes as the mobility of these dislocations decreases. This behavior occurs at cyclic stress amplitudes sufficiently small that the bulk deformation remains indistinguishable from linearly elastic. Measured values of microplastic strain (Section 2.2) are in essence determined by a product of the mobile dislocation density and a mobility factor. Ideally we would like to know these factors separately. An indentation hardness test provides a means to qualitatively characterize dislocation mobility. Microhardness progressively increases in Heat III material with fatigue in a manner illustrated in Fig. 20. It thus appears likely that localized hardening of

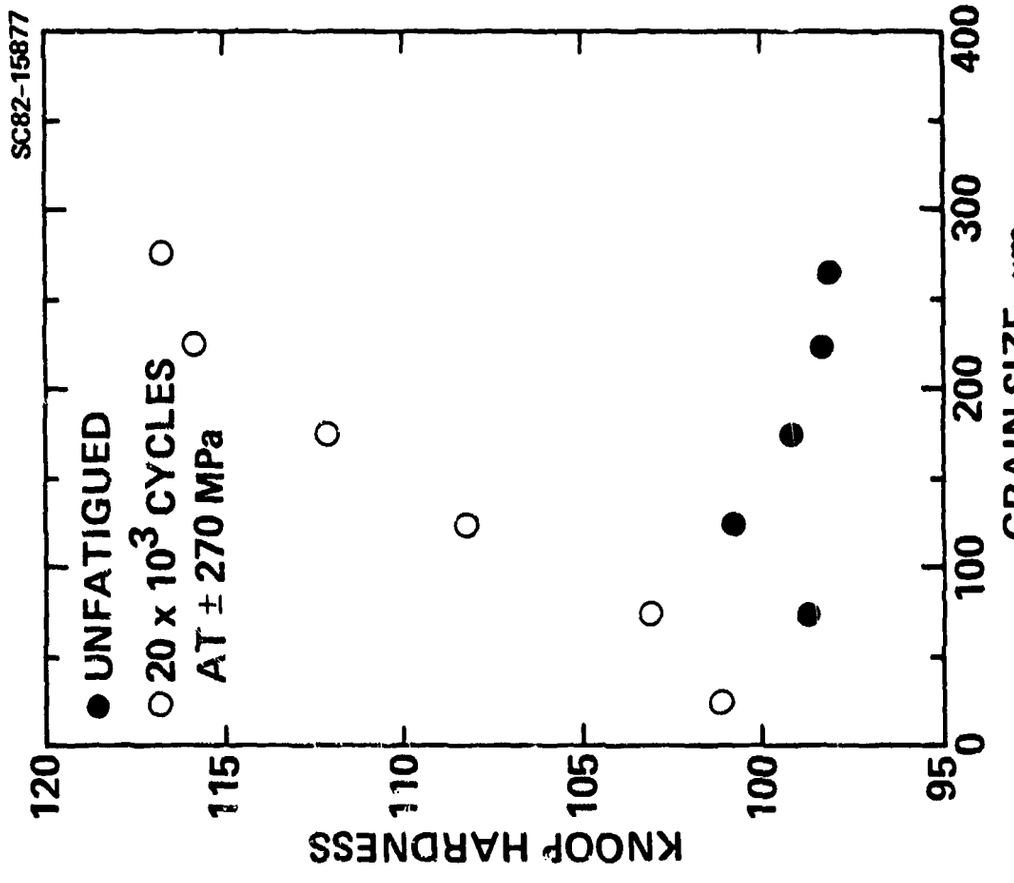

Fig. 20 Knoop hardness measurements vs grain size after a sample of Al 2219-T851 has been fatigued.

the surface begins early during fatigue in the 2219 alloy. Opening of the stress-strain hysteresis loop, then, occurs because the density of mobile dislocation is initially low and increases rapidly.

At least two stages of cyclic hardening of the surface must be considered. The microplasticity data indicate, for instance, that hydrogen increases the local hardness at plastic strain greater than 0.3%. This is the same trend as is observed in large strain experiments made using small surface cracks. However, we need to determine the effect of hydrogen hymidity on localized hardening of a thin layer of the surface as the localized microplasticity begins to develop. This can substantially effect the peak value of plastic strain developed during fatigue and thus impact crack initiation behavior. A method is discussed to characterize the quantity of interest by determining the effect of hardening on the dynamics of development of a new plastic zone as a surface crack tip begins propagation into a new surface grain.

2.3.2 Incubation

Frequently, the propagation of a surface crack is temporarily interrupted when a tip reaches the vicinity of a grain boundary. Several features of this phenomenon allow it to be recognized as resulting from a mechanism distinct from crack closure stress. For instance, incubation is observed even if the subsequent growth is crystallographic, in which case closure stress is unimportant because it is small [21]. Growth is completely stopped by the incubation mechanism, while it is frequently only slowed by closure stress. Moreover, the duration of incubation decreases substantially with increased amplitude of the cyclic stress, a result not expected from closure stress.

After a crack tip stops at a boundary, changes which precede renewed growth can be seen by measuring the crack tip opening displacement (CTOD) during progressive fatigue. We have done this for numerous cracks in Al 2219-T851, and find that if the growth into the next grain is non-crystallographic

it is preceded by a progressive increase in CTOD up to a critical value. This critical value increases linearly with the size of the grain at the crack tip [20]. An example of this behavior is given in Fig. 21, in which the plastic component of the opening displacement ($CTOD_p$) is plotted versus fatigue cycles. $CTOD_p$ is the measured CTOD minus the estimated elastic tip opening, which is taken as 10% of the opening $\delta(\sigma_{max})$ of the center of the crack [20]. The tip of the grain sized crack in Al 2219-T851 (Heat III) arrived at the boundary at 15×10^3 cycles, at which point the tip opening was elastic. With progressive fatigue $CTOD_p$ increased until growth recommenced at 35×10^3 cycles. We find that the later a crack tip arrives at a boundary, the longer is the average period of non-propagation. Frequently $CTOD_p \approx 0$ at the tips of the permanently stopped cracks.

Chang et al. [14] have proposed a model of incubation based on the following picture. Slip is confined between the crack tip and the grain boundary as growth procedes toward a boundary. Thus, when a crack tip first reaches a grain boundary, very little deformation in the new grain has taken place and $CTOD_p$ is initially small. Propagation into the new grain requires that an energy balance criterion derived by Cottrell [25] be met. For short cracks for which $\Delta K_{th} < \Delta K_o$, the plastic strain needed to achieve propagation accumulates as dislocations (of number n) are developed with cyclic loading in a slip band of length D in the next grain. We assume $CTOD_p \propto nD$. Chang et al. have proposed that the production of new dislocations in the band is driven by a local stress of the form $\sqrt{2c}(\tau - \tau_o - f(D)n)$ giving

$$\frac{dn}{dN} = C_1 D\sqrt{2c}\ (\tau - \tau_o - f(D)n) \quad . \tag{4}$$

C_1 is a material parameter, τ is a peak applied shear stress, 2c a crack length, and τ_o and $f(D)n$ are a friction stress and a back stress, respectively. For constant crack length, an expression for the duration of incubation can be obtained by integration of Eq. (4) and application of the Cottrell criterion. In a first order approximation there is no effect of back stress

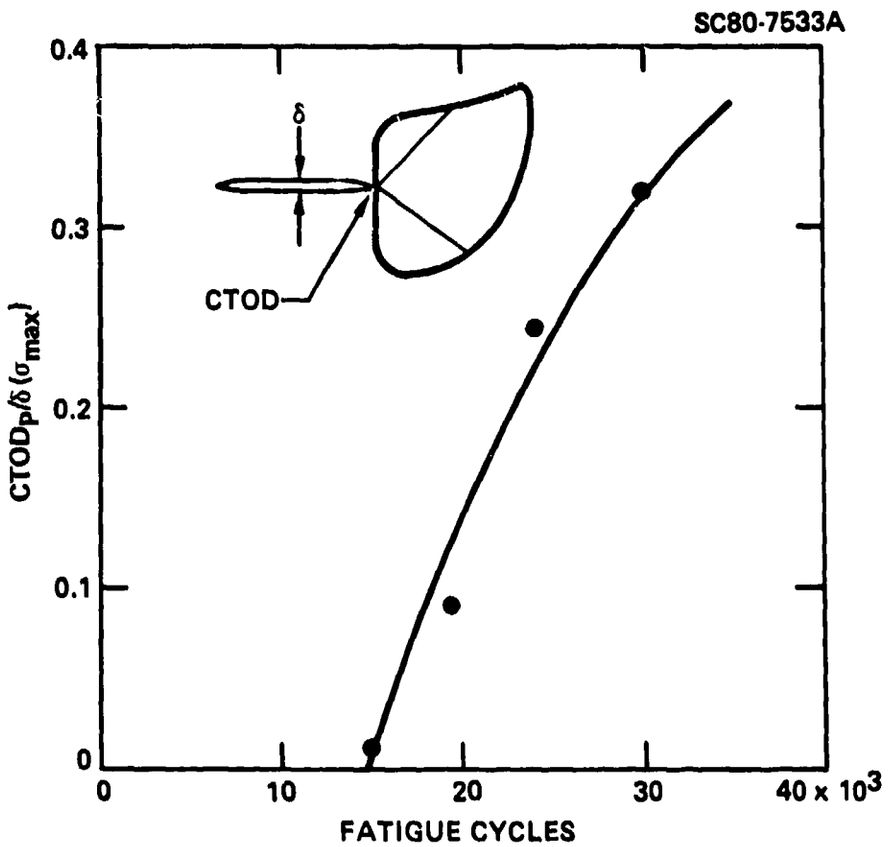

Fig. 21 Progressive increase in $CTOD_p$ for a crack tip which reached the grain boundary at 15×10^3 fatigue cycles in Al 2219-T851. Theoretical curve is from Eq. (8).

on incubation and the predicted duration of incubation does not increase with prior fatigue.

To rectify this discrepancy we hypothesize that the friction stress (τ_f) increases with fatigue from an initial value τ_o at a rate

$$\frac{d\tau_f}{dN} = \theta\,(\tau - \tau_f) \quad . \tag{5}$$

We present elsewhere [26] evidence that the surface of Al 2219-T851 cyclically hardens during fatigue. This justifies the trend but not the exact form of Eq. (5). The duration of non-propagation (ΔN_I) for a crack tip which arrives at a boundary at N_S fatigue cycles that one obtains depends on approximations made in applying the Cottrell criterion. We consider both 2c and η small, and assume that the net section stress rather than local stress is appropriately used in the Cottrell expression, and obtain

$$\eta \geq C_2/\tau \quad , \tag{6}$$

where C_2 is a material parameter. To derive an expression for ΔN_I we replace τ_o by τ_f in Eq. (4), integrate Eq. (5) to express τ_f as a function of τ_o and cycles N, neglect the back stress, integrate Eq. (4) between limits N_S and $N_S + \Delta N_I$ cycles and evoke Eq. (6) to obtain

$$\int_{N_S}^{N_S+\Delta N_I} \frac{C_1}{C_2} D\sqrt{2c}\;\tau(\tau - \tau_o)\, e^{-\theta N}\, dN = 1 \quad . \tag{7}$$

In like manner $CTOD_p \propto \eta D$ becomes

$$CTOD_p \propto D^2\sqrt{2c}\;(\tau - \tau_o)\left[e^{-\theta N_S} - e^{-\theta(N_S+\Delta N_I)}\right] \quad . \tag{8}$$

This representation of the interruption of growth by grain boundaries is presently under evaluation. As reported elsewhere [21] we have found for 2219 that cracks are stopped longer by small grains, consistent with this period being proportional to $D\sqrt{2c}$. $CTOD_p$ vs N data such as given in Fig. 21 appear to be adequately represented by Eq. (8). One adjustable coefficient has been used to obtain the curve shown in Fig. 22, but the departure from linearity is attributable to cyclic hardening of the surface, and the value of $\theta = 3.5\times10^{-5}$ cycles^{-1} used comes from an independent measurement [27] of θ from its effect on constituent particle fracture. Incubation has been observed in several aluminum alloys [28] in addition to 2219 including Al 6061-T6, Al 7075-T6 and Al 2024-T3. The effect of prior fatigue on the duration of interruption of growth is especially strong in the latter material. Results for Al 2024-T3 in Fig. 22 show that measured values of ΔN_I (normalized using $D\sqrt{2c}$) increase with N_S. These observations were made by repeated examination of stopped cracks at intervals during fatigue to determine ΔN_I. Results shown are for cracks with lengths nearly constant during fatigue and the lines in Fig. 22 are of the form

$$\ell n\,[\Delta N_I D\sqrt{2c}] + \ell n\,[\tau(\tau - \tau_o)C_1/C_2] = \theta N_S \quad , \tag{9}$$

an expression obtained from Eq. (7) for constant 2c. By fitting Eq. (9) to experimental data one obtains an estimate of a surface hardening coefficient at small plastic strains. In 2219, θ is a function of alloy hydrogen content and ambient humidity, as is discussed in Section 4.0.

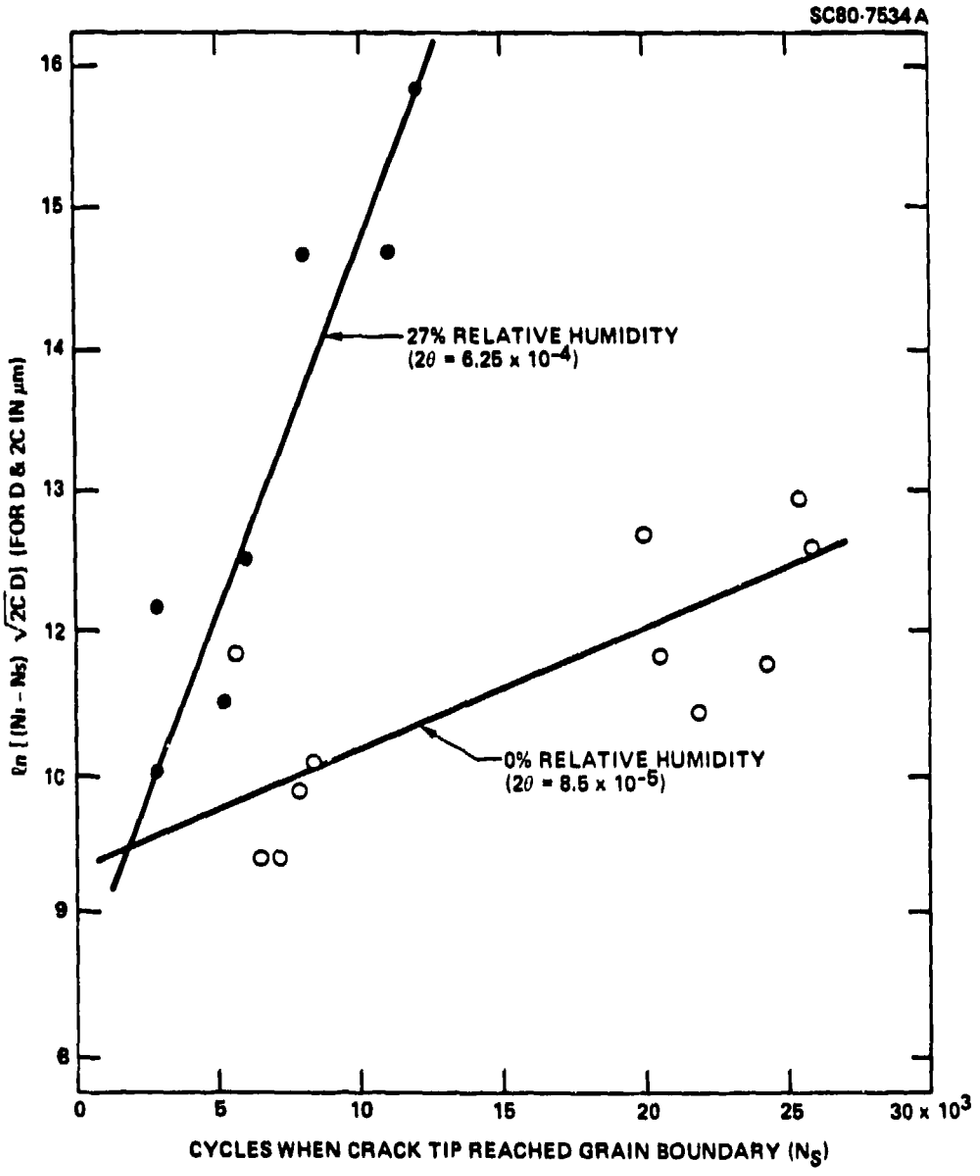

Fig. 22 Duration of incubation in Al 2219-T851 as a function of the cycles (N_S) required for crack tips to reach a grain boundary is longer in humid than in dry laboratory air and increases with N_S. Theoretical curve is from Eq. (9).

3.0 LOCALIZED PLASTIC DEFORMATION OF THE SURFACE - THE LARGE STRAIN CASE

3.1 Summary of Prior Results

Rice [29] suggested that the plastic component of crack tip opening displacement $CTOD_p \approx \varepsilon_y z_o/2$, where z_o is the size of the plastic zone and ε_y is the strain at the yield strength. For short surface cracks in aluminum alloys fatigued below the yield strength, z_o is the distance of the crack tip to the next grain boundary (Fig. 23). A measurement of $CTOD_p$ v z_o can therefore be used to obtain ε_y, a parameter which describes one facet of ductility. Results typical for Al 2219-T851 alloy are shown in Fig. 24. Parameters of short surface cracks are measured in the SEM using a jig which permits specimens to be loaded to the maximum tensile stress applied during fatigue (Fig. 4). Measurements made for each crack tip are illustrated in Fig. 23. We infer from results of an analysis by Green and Sneddon [30] that for an elastic crack (i.e., as $z_o \to 0$) $CTOD/\delta_{(\sigma max)} \approx 0.1$. The parameter $\delta(\sigma_{max})$ is the opening at the center of the crack and is approximately proportional to the crack length 2c. Thus with the normalization used in Fig. 24, all deformation above the dashed line is plastic. For convenience, we define a normalized strain ε_y' given by Eq. (10), which represents a normalized failure strain for the material in environment. The actual strain $\varepsilon_y \approx 0.0182\ \sigma_{max}\varepsilon_y'/\sigma_{yield}$. The proportionalty coefficient comes from the ratio of crack opening to crack length, which is only approximately known. Thus ε_y' is determinable with more accuracy than is ε_y. Further details are given in Ref. 28 and are to be published.

$$\varepsilon_y' = \frac{2c}{z_o}\ \frac{CTOD}{\delta(\sigma_{max})} - 0.1 \quad . \tag{10}$$

Values of ε_y' for Al 2219-T851 are discussed in Section 4.0.

SC80-7536

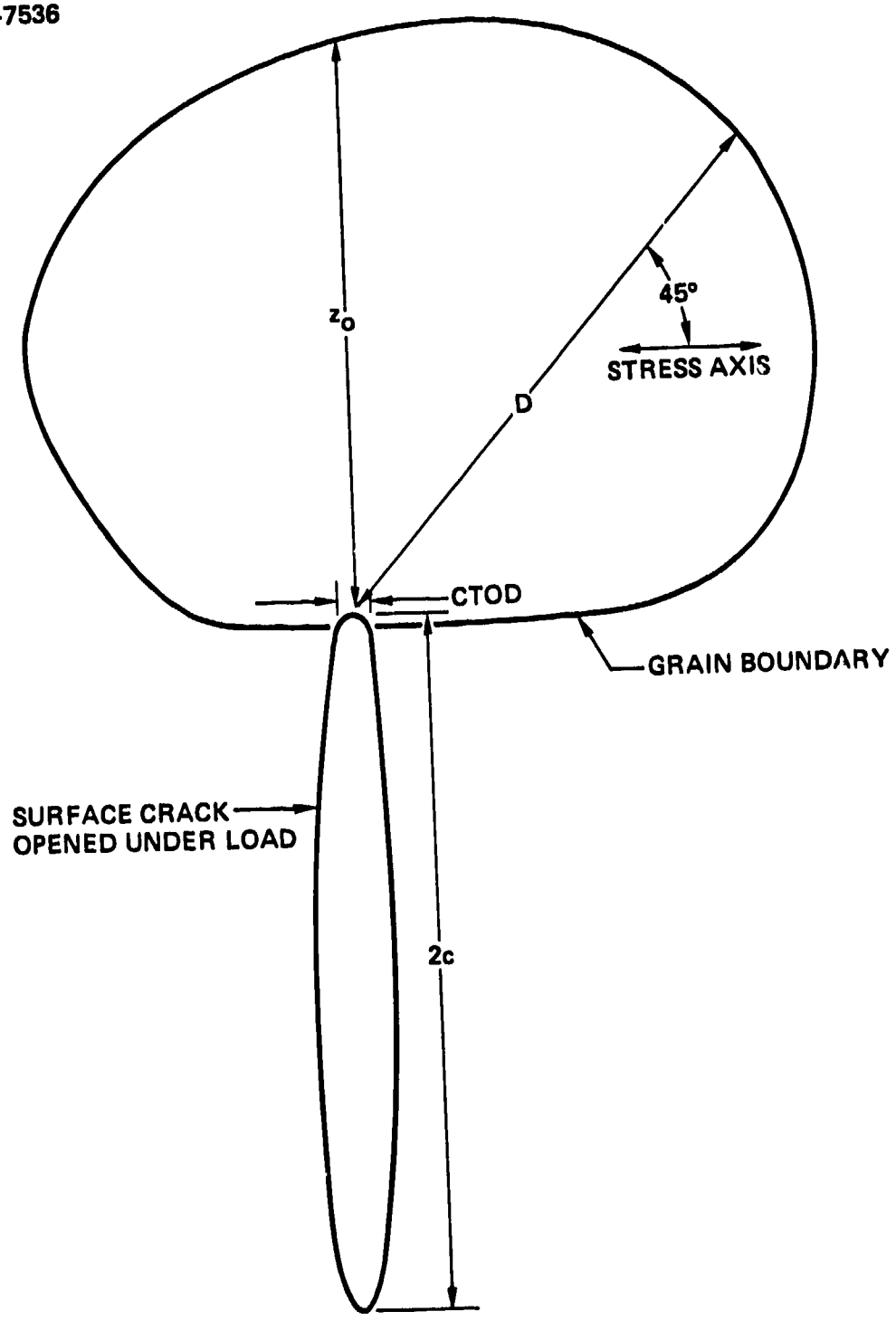

Fig. 23 Dimensional parameters used in determination of microplastic deformation. CTOP is found by extrapolation of displacements made near the tip to the tip as explained elsewhere [20].

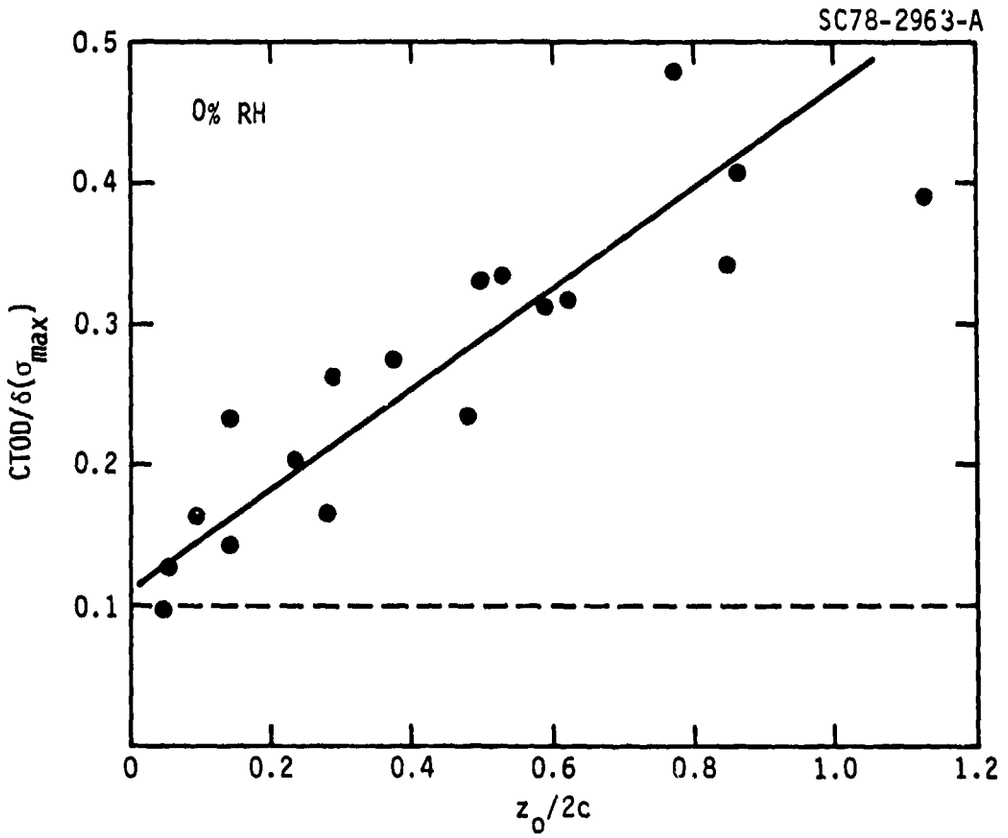

Fig. 24 Crack tip opening displacement vs distance z_0 of the crack tip to the next grain boundary for Al 2219-T851. With the normalization used a value of CTOD/$\delta(\sigma_{max})$ = 0.1 is the elastic component of the opening displacement. Plastic component increases with increased distance of crack tip to boundary. Dashed line is predicted elastic opening displacement.

4.0 DISCUSSION

Our results address three aspects of the properties of the surface of aluminum alloys subjected to fatigue in the bulk linearly elastic regime. These are: (1) the nature of the localized deformation at the surface, including the discovery of localized microplastic deformations of substantial magnitude; (2) the effect of ambient humidity and internal hydrogen on this plasticity; (3) and the relationship of localized plasticity to crack initiation and crack growth.

4.1 Localized Microplastic Deformation of the Surface of Al 2219-T851

Microplasticity measurements made within individual surface grains show that the surface of aluminum alloys can deform plastically while the subsurface remains elastic. The average strain in the surface is determined by the elastic constraints of the subsurface, and this is why conventional techniques are not able to measure the large amount of localized plasticity that takes place. At anyone time only a few surface grains sustain large tensile plastic strains, and these are offset by compressive elastic reactions in surrounding areas of the substrate. For Al 2219-T851 fatigued at ± 270 MPa the surface is initially elastic. With continued cyclic loading, the stress-strain hysteresis loop within individual grains first slowly opens and then begins to close. This process tends to occur first within grains having large surface cross-sections. We attribute the substantial scatter in the data to grain crystallographic orientation and to subsurface grain shape. In agreement with model of Chang et al. [14] and Tanaka and Mura [10], grain size is an important parameter in the development of microplasticity. These models attribute the progressive opening of the local stress-strain hysteresis loops to the production of new mobile dislocations on each loading cycle in a number proportional to the grain size. Neither model considers the effect of cyclic hardening of the individual grains, which is apparently responsible for closing of the loops with sustained fatigue. An phenomonological representation of the localized microplastic deformation of the surface which includes

descriptions of both the development of localized plastic strain and hardening to the elastic state are discussed elsewhere [15].

4.2 Effects of Ambient Humidity and Internal Hydrogen on Surface Local Microplastic Behavior

Summarized in Table 4 are the effects of ambient hyumidity and internal hydrogen on the mechanical properties of the surface of Al 2219-T851.

Table 4

Effect of Environment on Surface Mechanical Properties

	Low Strain				High Strain	
	α (μm^{-1})*		θ ($cycle^{-1}$)		ε'_y	
Hydrogen Content	Dry Air	Moist Air	Dry Air	Moist Air	Dry Air	Moist Air
Heat III (Low H)	1.73×10^{-5}	0.6×10^{-5}	1×10^{-5}	3.5×10^{-5}	0.37	0.29
Heat II (High H)	-	2.97×10^{-5}	$< 1 \times 10^{-6}$	$< 1 \times 10^{-6}$	0.29	0.27

*for 20,000 cycles at ± 270 MPa

The response of the surface to environment is divided into small plastic (< 0.5%) and large plastic strain (>> 1%) cases. Parameters α, θ, and ε'_y describe various aspects of the mechanical properties of the surface which are environmentally sensitive. Presently, they must be treated as empirical coefficients, although their qualitative relationships to more fundamental parameters are partially understood.

The rate at which new mobile dislocations are developed by fatigue increases with the α value of a material. At small plastic strains localized hardening of the surface is manifest by the progressive reduction with fatigue

in the rate of crack growth across grain boundaries. Parameter θ (and Eq. (7)) describes this behavior. Large values of θ are associated with less dislocation mobility and larger periods of no growth of surface cracks at grain boundaries. The same parameters appears in two other models which require an accurate calculation of the peak tensile local plastic strains which develop at a surface. In both cases the predicted values of fatigue induced surface plasticity are larger than observed, if cyclic hardening of the surface is excluded from the model [15,27].

Parameter ε_y' describes the local ductility of the alloy matrix at the large plastic strains associated with fatigue crack tips. Trends in this quantity with environment are similar to those seen in measured residual strain, obtained by the reference gauge technique, after substantial cyclic hardening of the surface has taken place. Clearly, the local hardening of individual surface grains is a complex process for which θ and ε_y' represent performance only in the limiting cases of small and large plastic strains respectively.

The observed effects of internal hydrogen and of ambient environment on α, θ and ε_y' are rationalized as follows. At small plastic strains internal hydrogen increases the rate of buildup of localized values of the tensile plastic deformation sustained within an individual grain on each tensile loading cycle. Apparently hydrogen decreases the rate of early cyclic hardening of the surface. The large local ductility of hydrogen charged 2219 indicates that hydrogen also increases the rate at which new mobile dislocations are formed on each loading cycle. In low hydrogen content aluminum, ambient humidity decreases localized surface microplasticity over that in dry air. This is opposite to the effect of internal hydrogen, and is evidence that at small plastic strains the hydrogen from the water vapor does not significantly effect the mechanical properties of the surface. We think this is probably because of the limited diffusion of hydrogen across the surface oxide barrier. Instead, it can be argued, as previously noted by Grosskreutz [4], that

the surface oxide effects subsurface dislocation mobility leading to reduced ductility at small strains.

For large plastic strains it is apparent that hydrog . from either internal or external sources reduces the local ductility of the surface. This suppresses further crack initiation but accelerates short crack growth rates. Similar effects of hydrogen have been found in iron and nickel alloys, although at much larger hydrogen contents than at the less than 1 ppm important to aluminum [22,23].

No consensus has been reached on the underlying mechanism of the activity of the hydrogen. Heubaum and Birnbaum suggest that hydrogen may change the degree of screw character in the dislocation motion at low plastic strains [22]. M. Fine [31] has recently suggested that solid solution softening of the surface in the presence of small amounts of hydrogen might explain the observations. We think this interpretation merits further consideration.

4.3 Relationship of Localized Plasticity to Crack Initiation and Growth

Rates of consituent particle fracture in 2219 are derived by using a single value of fracture surface energy for all environments. The substantial effect of internal hydrogen and water vapor on number of particles broken by fatigue are predictable from the changes which are induced in the peak tensile plastic deformation within individual grains at the surface.

Hydrogen reduces the ductility of the aluminum matrix at surface crack tips. Crack closure stresses associated with crack tip plasticity are decreased and the propagation rates are increased by this change in ductility. While rigorous experiments remain to be completed, it appears that the only important effect of the hydrogen on short crack growth in 2219 is to change the closure stress by altering plasticity. There is no evidence that hydrogen changes the local fracture strength of the material at the crack tip. A

similar conclusion can be reached from studies reported by Buck et al. [32] for long cracks in Al 7075-T6 alloy.

Heat to heat variations in the hydrogen content of commercial aluminum alloys is sufficient to substantially effect alloy lifetime. In addition, grain size, and the distribution in constituent particle sizes in alloys are important parameters effecting lifetime. Figure 25 shows a comparison of predicted and measured distributions in fatigue lifetimes of Al 2219-T851 alloy obtained using Rockwell IR&D funds. Predicted values are from a Monte Carlo simulation [33] of crack initiation and crack growth in computer simulated smooth bar specimens fatigued at a cyclic stress amplitude of ± 270 MPa. This simulation incorporates models [21] which utilize parameters derived from the environmental studies reported here. A statistical distribution in lifetimes is obtained by repeated operation of the simulation for bars of different local microstructure (i.e., in local grain size, and the size and location of constituent particles they contain), obtained by random selection from experimentally measured distributions in the microstructural quantities [18]. Materials A and C demonstrate for fixed hydrogen content that the predicted effect of decreasing grain size from 60 to 30 μm is to increase the alloy fatigue lifetime for fatigue at ± 270 MPa. For the two commercial alloys used in this study both alloy grain size and hydrogen content are variables. Heat II, which has the smaller grain size and higher hydrogen content, has a shorter fatigue lifetime than does Heat III. Both the Monte Carlo simulation and experiment show that hydrogen content is the more important parameter. Hydrogen shortens fatigue lifetime by increasing the local ductility of the alloy matrix at the surface during fatigue, thus accelerating crack initiation; and by decreasing crack tip ductility during growth, lowering the crack closure stress and accelerating the early crack growth rates.

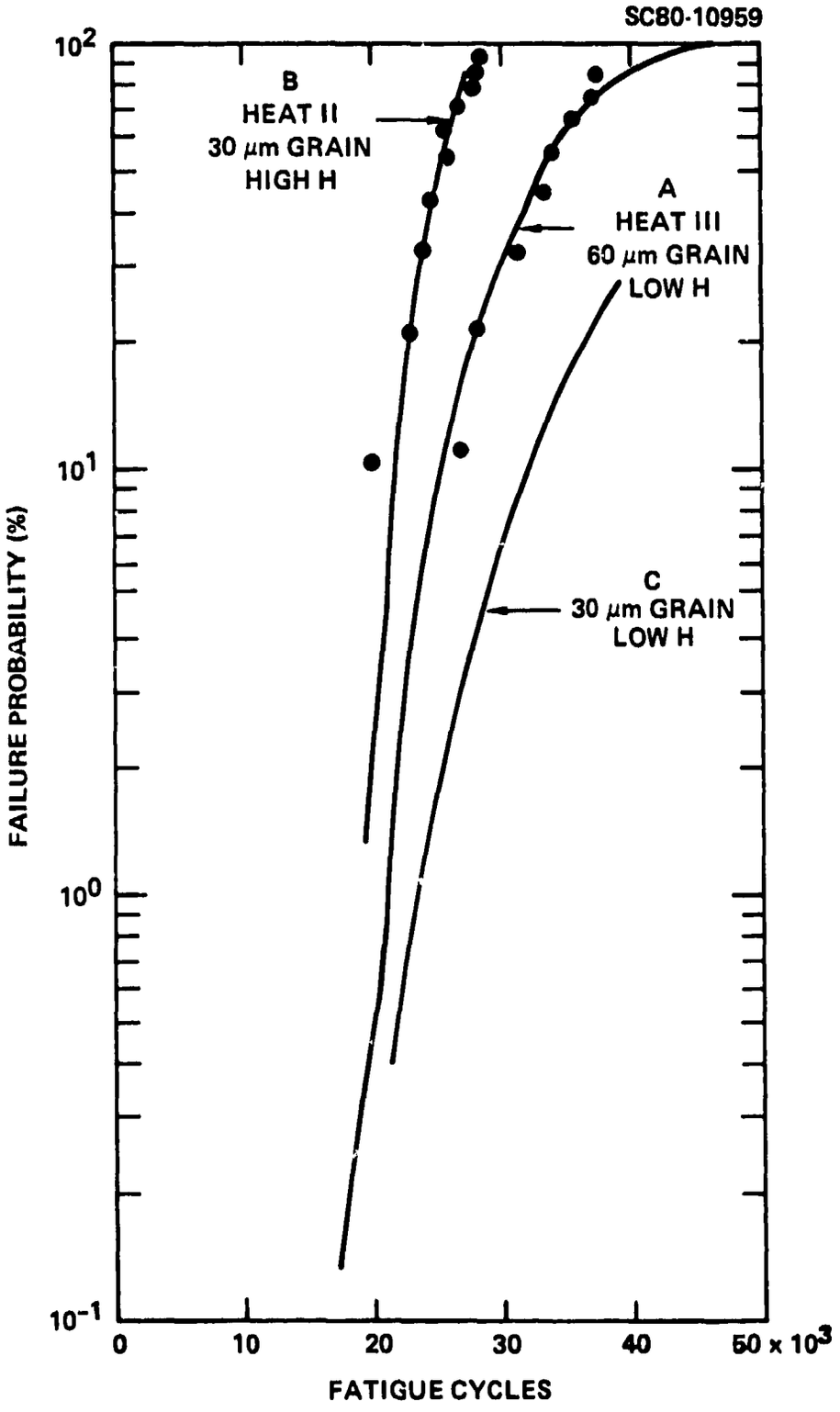

Fig. 25 Effect of alloy grain size and hydrogen content on the scatter in lifetime for three cases. Data are from smooth bars, and curves are obtained by a Monte Carlo simulation of crack initiation and growth for 1000 simulated fatigue specimens of each material.

5.0 CONCLUSIONS

1. Localized plastic deformation of Al 2219-T851 occurs within individual surface grains during fatigue, even if the bulk loading is linearly elastic. Initially the surface deformation is also elastic, but with repeated cyclic loading plastic strains within a large grain, on a single tensile cycle, can exceed 0.5%.

2. The rate at which the localized plasticity developes and the peak strains attained on any cycle are extremely sensitive to both internal hydrogen content (at < 1 ppm) and to atmospheric humdity. Internal hydrogen increases the initial rate at which the local stress-strain loops open with fatigue. Atmosphere humidity decreases the rate of loop opening from that measured in dry air.

3. Constitutent particles at the surface are fractured at a critical value of peak tensile local plastic strain. The strong effect of environment on particle fracture comes from its effects on the local ductility of the matrix material within individual grains at the surface.

4. At the large plastic strains associated with short surface crack propagation, hydrogen from either internal or external (humidity) sources decreases the ductility of material at the crack tip and accelerates crack growth rates.

6.0 REFERENCES

1. J.K. Tien, A.W. Thompson, I.M. Bernstein and R.J. Richards, "Hydrogen Transport by Dislocations," Met. Trans. 7A, 821 (1976).

2. R.J. Richards, S. Purushothaman, J.K. Tien, J.D. Frandsen and O. Buck, "Kinetics of Environmental Fatigue Crack Growth in a Nickel-Copper Alloy: Part II. In Hydrogen," Met. Trans. 9A, 1107 (1978).

3. O. Buck, L.A. Ahlberg, L.J. Graham, G.A. Alers, J.A. Wert, M. Amano, "Effects of Hydrogen on Elastic and Physical Properties of Niobium," Proceedings of the 6th International Conference on Internal Friction and Ultrasonic Attenuation in Solids, ed. by R.R. Haseguti and N. Mikoshiba, Univ. of Tokyo Press, 407-411 (1977).

4. J.C. Grosskreutz, Surface Science, 8, 173 (1967).

5. D.J. Duquette, private communication.

6. W.L. Morris, R.V. Inman and M.R. James, J. Materials Science 17 (1982).

7. W. L. Morris, M. R. James, and O. Buck, Met. Trans., 12A (1981) 57.

8. S. Taira, K. Tanaka and Y. Nakai, Mech. Res. Comm., 5 (1978) 375.

9. W. L. Morris and M. R. James, Met. Trans., 11A (1980) 850.

10. K. Tanaka and T. Mura, Met. Trans. 13A, 117 (1982).

11. D. L. Davidson and J. Lankford, Trans. ASME-J. Eng. Matls. and Tech., 98H (1976) 24.

12. D. R. Williams, D. L. Davidson and J. Lankford, Expt. Mech., 20 (1980) 134.

13. R. N. Pangborn, S. Weissman and I. R. Kramer, Met. Trans., 12A (1981) 109.

14. R. Chang, W. L. Morris and O. Buck, Scripta Met., 13 (1979) 191.

15. M. R. James and W. L. Morris, "The Fracture of Constituent Particles During Fatigue," accepted by Matls. Sci. and Eng.

16. N. T. Thompson, N. J. Wadsworth and N. Louat, Phil. Mag., 1, 113 (1956).

17. I. R. Kramer, Met. Trans., 5A, 1735 (1974).

18. W. L. Morris and M. R. James, "Statistical Aspects of Fatigue Failure," in Quantitative Measurement of Fatigue Damage, Conf. Proceedings, Dearborn, MI, May 10-11, 1982, ASTM STP, to be published.

19. Abdelfattah Elkholy, Jacques Galland, Pierre Axou and Paul Bastien, C. R. Acad. Sc. Paris, 284, 363 (1977).

20. W. L. Morris, Met. Trans., 9A, 1345 (1978).

21. W. L. Morris and M. R. James, Met. Trans., 11A, 850 (1980).

22. F. Heubaum and H. K. Birnbaum, "The Effect of Hydrogen on the Fracture and Slip Behavior of Nickel," ONR Technical Report, Contract USN 00014-75-C-1012 (March 1981).

23. H. Kimura, H. Matsui, A. Kimura, T. Kimura and K. Oguri, in Hydrogen Effects in Metals, ed. I. M. Bernstein and A. W. Thompson, AIME, Warrendale, PA, 191 (1981).

24. J. P. Hirth, Met. Trans., 11A, 861 (1980).

25. A.H. Cottrell, AIME Met. Trans. 212, 192 (1958).

26. W.L. Morris, M.R. James and O. Buck, Nondestructive Evaluation: Microstructural Characterization and Reliability Strategies, O. Buck and S.M. Wolf, eds., AIME, 387 (1981).

27 M.R. James and W.L. Morris, Residual Stress for Designers and Metallurgists, L.J. VandeWalle, ed., ASM, Metals Park, OH, 169 (1981).

28 W.L. Morris, M.R. James, O. Buck, R. Chang and J.W. Wert, "Mechanisms by Which Humid Alters Ductility," Tech. Report, April 15, 1979-1980, ONR Contract No. N00014-79-C-0334.

29 J.R. Rice, Fatigue Crack Propagation, ASTM STP 415, Am. Soc. for Testing and Materials, 247 (1967).

30. A.E. Green and I.N. Sneddon, Proc. Cambridge Phil. Soc., 46, 159 (1950).

31. M. Fine, private communication.

32. Buck et al.

33. W.L. Morris, M.R. James and O. Buck, Eng. Fract. Mech., 13, 213 (1980).

7.0 LIST OF PUBLICATIONS

1. W.L. Morris, M.R. James, O. Buck, R. Chang, J.A. Wert, Mechanisms by Which Hymidity Alters Ductility, Technical Report for period 4/15/79-4/14/82, Contract No. N00014-79-C-0334.

2. W.L. Morris, M.R. James and R.V. Inman, Mechanisms by Which Humidity Alters Ductility, Technical Report for period 4/15/80-4/14/81, Contract No. N00014-79-C-0334.

3. W.L. Morris, R.V. Inman and M.R. James, "Measurement of Fatigue Induced Surface Plasticity," J. Mat. Science (In Press).

4. M.R. James and W.L. Morris, "Fatigue of Constituent Particles During Fatigue," Mat. Sci. Eng. (In Press).

5. W.L. Morris and M.R. James, "Statistical Aspects of Fatigue Failure," to be published in Proceedings of the International Conference on Quantitative Measurement of Fatigue Damage, J. Lankford, ed., Dearborn, Mich. May (1982).

6. M.R. James and W.L. Morris, "The Role of Microplastic Deformation in Fatigue Crack Initiation," to be published in Proceedings of the International Conference on Quantitative Measurement of Fatigue Damage, J. Lankford, ed., Dearborn, Mich. May (1982).

8.0 LIST OF PRESENTATIONS

1. W.L. Morris and M.R. James, "Statistical Aspects of Fatigue Failure," at the International Conference on Quantitative Measurement of Fatigue Damage, Dearborn, Mich. May (1982).

2. M.R. James and W.L. Morris, "The Role of Microplastic Deformation in Fatigue Crack Initiation," at the International Conference on Quantitative Measurement of Fatigue Damage.

STATISTICAL ASPECTS OF FATIGUE FAILURE

W.L. Morris and M.R. James

Rockwell International Science Center
1049 Camino Dos Rios
Thousand Oaks, California 91360

The elements of a methodology to calculate the scatter in fatigue lifetime of alloys are described. Lifetime variations, which arise from differences in microstructure from specimen-to-specimen of a uniform heat of material and from differences in alloy grain size and in mechanical properties from heat-to-heat are treated. The models are formulated for certain structural aluminums for which the dominant mode of crack initiation is by fracture of constituent particles at the surface. However, the techniques should be extendable to other structural materials.

Fatigue lifetime is predicted by combining models of crack initiation and of short crack growth to develop a Monte Carlo simulation of the failure process on a microscopic level. Predicted statistical fluctuations in lifetime arise in the model from small random differences in the size and shape of grains in the vicinity of sites of crack initiation and from variations in the size of constituent particles and in their location relative to the grain boundaries. Crack initiation and growth models are described, and results which test predictions of microscopic cracking behavior are presented. The models fall into three classes.

Intermediate growth concerns propagation of short cracks, typically two to ten grain diameters long, for which linear elastic fracture mechanics (LEFM) must be slightly modified to accurately predict propagation rate. At least one parameter in addition to cyclic stress intensity (ΔK) is required. Models are presented for cases in which the fracture surface roughness changes with crack length, thereby modifying the cyclic stress intensity factor, and in which an elastic-plastic correction to LEFM must be made to account for large plastic zone size. Two other examples are given in which intermediate growth behavior is affected by the interruption of growth by grain boundaries.

Early growth concerns the propagation of cracks of approximately the grain size. Propagation of such cracks is substantially affected by grain boundaries in structural aluminums, and LEFM must be modified severely to predict growth rate from the microstructure in the crack path. The blockage of growth of surface cracks in Al 2219-T851, and Al 7075-T6 is demonstrated by plotting the relative location of surface crack tips, which are found to be clustered at the boundaries. Two mechanisms that contribute to this phenomenon are analyzed in detail. Incubation is the requirement that the material at the crack tip be plastically deformed before growth begins into the next grain. We show for a Al 2024-T3 alloy that the duration of non-propagation from incubation increases as the surface cyclically hardens during fatigue. Crack closure stress arising from crack tip plasticity fluctuates with plastic zone size which is controlled by grain boundary constraints in Al 2219-T851. Rates of propagation of surface cracks in the 2219 alloy are predicted from the size and shape of grains in the crack path, using empirical models of incubation and closure stress.

Crack initiation at constituent particles is more probable in large particles contained within large grains. Models of this phenomenon are discussed and predicted, and measured numbers of particles fractured by fatigue in Al 2219-T851 are compared.

Models of crack initiation and growth are combined to predict the fatigue lifetime of smooth bars of two heats of Al 2219-T851. These differ in grain size and in as-received internal hydrogen content. Results are shown in Fig. 1, where the dots are experimental data and the curves are from a Monte Carlo simulation. It is the hydrogen in alloy B which reduces fatigue lifetime compared to the larger grain size alloy A. Alloy C is a hypothetical material having the grain size of B, but no internal hydrogen. We conclude the paper with a discussion of the implications of the statistical aspects of the microscopic failure process to prediction of early fatigue failure.

ACKNOWLEDGEMENTS Incubation was studied under contract No. N00014-79-C-0334 supported by ONR. Rockwell International IR&D funds supported the remainder of the research.

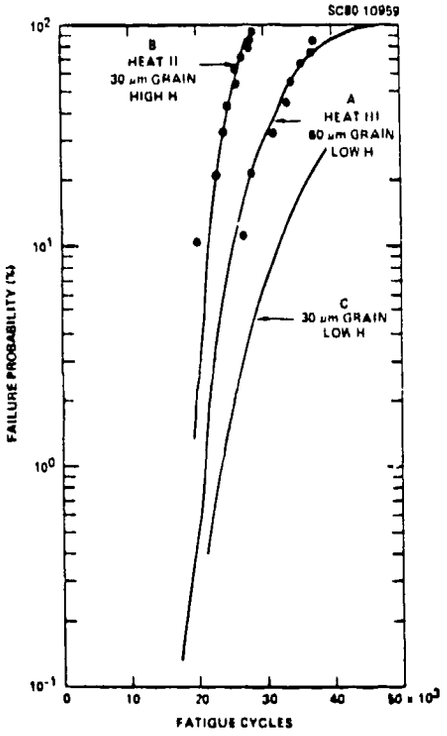

Fig. 1 Comparison of predicted and measured distribution in the lifetime of smooth bars of Al 2219-T851 fatigued at ± 270 MPa.

THE ROLE OF MICROPLASTIC DEFORMATION IN FATIGUE CRACK INITIATION

M.R. James and W.L. Morris
Rockwell International Science Center
Thousand Oaks, CAS 91360

Environmental humidity and internal hydrogen are shown to alter the number of constituent particles which fracture on the surface of Al 2219-T851 specimens during fatigue. The role of localized microplastic deformation of the surface in this crack initiation process is determined by measuring fatigue induced plastic strains within individual grains. It is shown that the microplastic strains are altered by humidity and internal hydrogen content in a manner consistent with their effects on particle fracture. A simple model based on a strain energy criterion for particle fracture is proposed to relate the measured local strains to the numbers and sizes of particles which fracture during fatigue. The model is used to predict the percentage of particles in the Al 2219 alloy which fracture as a function of the size of the grain in which they are contained.

The plastic strains were measured over a gauge length of 20-40 μm by placing small flakes of mica on the surface of specimens after fatigue [1]. Scanning electron microscopy was used to measure load induced changes in the distance between points on the alloy substrate by using the mica as a reference. The plastic strain, $\Delta\varepsilon_r$, was measured over a tensile loading cycle and is the sum of the local plastic strain in the grain and the compressive elastic reaction induced by the surrounding grains; in effect, $\Delta\varepsilon_r$ is a residual strain. The gauge length of approximately 40 μm was chosen to enable accuracies of ± 0.005% strain to be obtained, but yet to be small enough to allow measurements within individual grains. This made it possible to obtain a relationship between $\Delta\varepsilon_r$ and the distance of slip between grain boundaries at each measurement site. $\Delta\varepsilon_r$ was found to increase more rapidly during fatigue at sites of large slip for specimens fatigued at 75% of the monotonic yield strength.

Atmospheric humidity reduced the peak plastic strains achieved during fatigue of 2219 as compared to dry air. A small amount of internal hydrogen (at contents less than 1 ppm) increased the development of localized plasticity at plastic strains less than 0.3%. This shows clearly that the effect of humidity on the small plastic strains important to crack initiation does not come from hydrogen embrittlement of the matrix. Later in fatigue, cyclic hardening leads to decreased plasticity within the larger grains at the surface.

The strain important to particle fracture is the peak tensile plastic strain $\Delta\varepsilon_{pmax}$. At N fatigue cycles, $\Delta\varepsilon_{pmax}$ can be estimated from measured values of $\Delta\varepsilon_r$ by assuming that $\Delta\varepsilon_{pmax}$ is proportional to the peak value of $\Delta\varepsilon_r$ experienced at any cycle prior to N. Since $\Delta\varepsilon_r$ is dependent on the particle to grain boundary slip distance, D, we can write an empirical relationship

$$\Delta\varepsilon_{pmax} = \alpha(N)D \quad . \tag{1}$$

$\alpha(N)$ is determined from $\Delta\varepsilon_r$ data and varies with internal hydrogen content of the alloy.

The minimum size, w_{min}, of constituent particle which can be fractured by a local strain of $\Delta\varepsilon_{pmax}$ is calculated from a strain energy criterion for fracture. We equate the strain energy in a particle of diameter w_{min} with the energy required to produce the fracture surface and obtain

$$w_{min} = \frac{\beta}{\Delta\varepsilon_{pmax}^2} \quad . \tag{2}$$

Parameter β is related to the fracture surface energy which is unknown. A single value of β was selected to describe all Al 2219-T851 alloys in both humid and dry environments.

Equations (1) and (2) are applied to predict the percentage of particles fractured by fatigue in 2219. One comparison of predicted and measured values is presented in Fig. 1 as a function of D, for an alloy rich in internal hydrogen. Such comparisons are made for several combinations of alloy hydrogen content and environmental humidity. We conclude that the substantial effect of these factors on the number of particles broken during fatigue is due to their direct effect on the microplastic properties of the alloy surface.

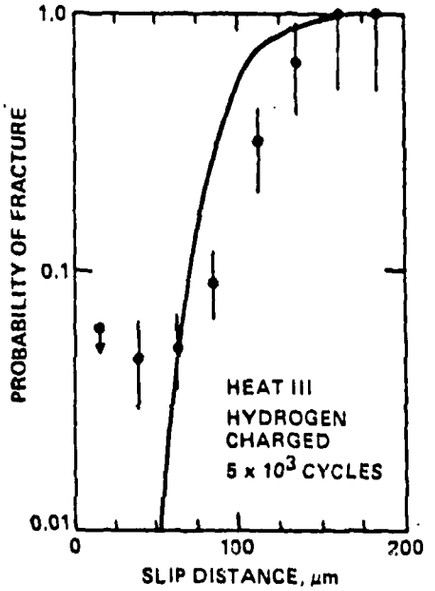

Fig. 1 Probability of a particle being fractured versus slip distance for hydrogen charged Al 2219-T851. The data (solid circles) are plotted as a histogram over 25 μm intervals in slip distance. The solid curve is predicted by Eq. (2).

Acknowledgements

This research was supported by the Office of Naval Research under Contract No. N00014-79-C-0334.

Reference

1. W.L. Morris, R.V. Inman and M.R. James, "Measurement of Fatigue Induced Surface Plasticity," accepted by J. Matls. Science.